

# Accurate evaluation of parameters of lattice clocks

Andrei Derevianko\*

*Physics Department, University of Nevada, Reno, Nevada 89557-0058*

Sergey G. Porsev

*Petersburg Nuclear Physics Institute, Gatchina, Leningrad district, 188300, Russia  
and Physics Department, University of Nevada, Reno, Nevada 89557-0058*

(Dated: April 11, 2007)

A theoretical background for evaluating various atomic-structure parameters affecting performance and ultimate accuracy of the lattice-based atomic clocks is presented. We evaluate a number of properties such as the hyperfine-induced transition width of the clock transition, multipolar and vector dynamic polarizabilities, static polarizabilities, “magic” trapping wavelengths, hyperfine-induced g-factors, and black-body radiation shifts. Numerical estimates are given for a number of divalent atoms presently under investigation, with a particular emphasis on ytterbium clock. The numerical values are obtained with accurate relativistic many-body techniques.

PACS numbers: 06.30.Ft, 32.80.Pj, 31.15.Ar

## I. INTRODUCTION

Atomic clocks based on ultranarrow  ${}^3P_0 - {}^1S_0$  transition in divalent atoms may offer a new level of time-keeping accuracy. In addition, they may facilitate tracking changes in fundamental constants over time, measuring gravitational red shifts, and timing pulsars. Compared to microwave atomic clocks, such as the present-day Cs frequency standard, the optical clocks have an advantage that optical transitions have a much higher frequency and potentially much higher resonance quality factors.

In the Katori scheme [1] (see Chapter XXX **Editor, please insert cross-reference**), ultracold atoms are confined in an optical lattice, largely eliminating Doppler and recoil shifts. The lattice laser wavelength is selected in such a way that the dominant perturbation of the clock frequency, the induced AC Stark shifts, for both clock states exactly cancel. At this “magic” wavelength of the lattice laser, the clock frequency is relatively insensitive to laser polarization and power. Although other effects still perturb the clock frequency, estimates [2, 3] indicate that the projected fractional uncertainty of such clocks may be as low as  $10^{-18}$ . By comparison, a few  $10^{-16}$  is the fractional uncertainty of the current Cs standard realizing the SI definition of the unit of time. This advantage of the optical-lattice clocks has motivated a number of recent proposals: the original Katori’s scheme [1] with fermionic Sr isotopes has been extended to Mg [4], Ca [5], and Yb [3] atoms and to bosonic isotopes [6, 7]. In addition, various schemes of probing the highly-forbidden  $nsnp\,{}^3P_0 - ns^2\,{}^1S_0$  clock transition have been proposed: three-photon transition, electromagnetically-induced transparency, and transition assisted by magnetic field [6–8].

While most of these developments will be reviewed in other chapters of this book, the goal of this chapter is to provide a rigorous theoretical background for evaluating various atomic-structure parameters affecting performance and ultimate accuracy of the lattice-based atomic clocks. We start by giving an introduction to the correlation problem for divalent atoms in Section II. In that Section we also describe a relativistic many-body code used in our calculations and demonstrate its capabilities by computing energies, dipole-matrix elements, hyperfine-structure constants and static polarizabilities. We further evaluate parameters of the lattice-based clocks: the magic wavelengths and multipolar polarizabilities (Sec. III), hyperfine-induced natural width of the clock transitions (Sec. IV), vector polarizabilities (Sec. V), hyperfine-induced electronic magnetic moments (g-factors, Sec. VI), and black-body radiation shifts (Sec. VII). Numerical estimates are given for a number of divalent atoms presently under investigation, with a particular emphasis on ytterbium clock.

Unless specified otherwise, we use atomic units ( $|e| = \hbar = m_e \equiv 1$ ) throughout this chapter. In these units, the speed of light  $c = 1/\alpha$ , where  $\alpha \approx 1/137$  is the fine-structure constant. We use the Gaussian electromagnetic units. Temperature is expressed in units of  $E_h/k_B$ , where  $E_h$  is the Hartree (atomic unit of energy) and  $k_B$  is the Boltzmann constant.

---

\*Electronic address: [andrei@unr.edu](mailto:andrei@unr.edu)

## II. SOLVING ATOMIC MANY-BODY PROBLEM

The clockwork in lattice clocks takes advantage of the electronic structure of atoms with two valence electrons outside a closed-shell core. Such systems include group II atoms, such as magnesium, calcium, and strontium, or more complex divalent atoms such as ytterbium and mercury atoms. A typical level structure of such atoms is shown in Fig. 1. The clock transition is between the ground  $ns^2\ ^1S_0$  state and the  $J = 0$  component of the lowest-energy triplet state fine-structure manifold,  $nsnp\ ^3P_J$ . In the following presentation we will also need nuclear parameters for the stable isotopes; these are compiled in Table I.

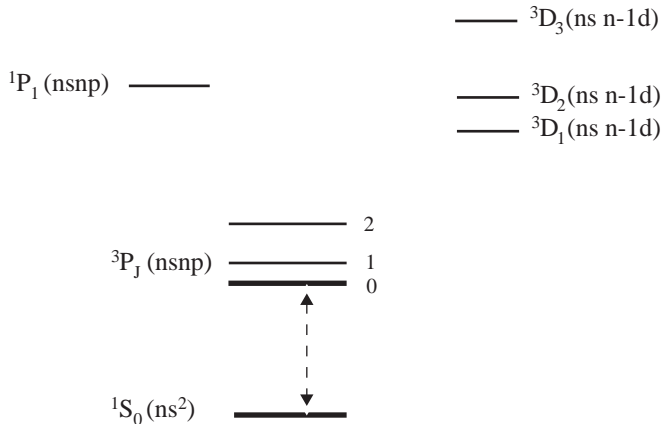


FIG. 1: A diagram of the low-lying energy levels for Mg ( $n=3$ ), Ca ( $n=4$ ), Sr ( $n=5$ ), and Yb ( $n=6$ ). The relative position of the levels above the  $^3P_J$  fine-structure manifold depends on the atom. This diagram reflects the Yb energy levels (the core-excited states are not shown). The clock transition is between the ground and the lowest-energy  $^3P_0$  state.

TABLE I: Nuclear parameters of the stable fermionic isotopes of Mg, Ca, Sr, and Yb. Here  $I$  are the nuclear spins and  $\mu_I/\mu_N$  are the nuclear magnetic moments expressed in units of the nuclear magneton  $\mu_N$ .

Isotope	$I$	$\mu/\mu_N$
$^{25}\text{Mg}$	$5/2$	-0.85546
$^{43}\text{Ca}$	$7/2$	-1.31727
$^{87}\text{Sr}$	$9/2$	-1.09283
$^{171}\text{Yb}$	$1/2$	0.4919
$^{173}\text{Yb}$	$5/2$	-0.6776

Most of the enumerated atoms are relatively heavy and the relativistic effects play an important role (for example, the nuclear charge of Hg is  $Z = 80$ ). Moreover, certain properties, e.g., hyperfine-induced decay rates depend on the wave functions near the nucleus where the relativistic effects dominate. Because of this relativistic nature of the problem, below we present a theoretical analysis that is uniformly based on the Dirac equation and *ab initio* relativistic methods of atomic structure. In most cases we reduce the derived expressions to the more familiar nonrelativistic formulas.

In addition, an accurate description of the atomic structure of the heavy neutral divalent atoms requires treating the correlation problem. A variety of atomic-structure methods has been developed since the inception of quantum mechanics. One of such methods is the multiconfiguration Hartree-Fock method with relativistic effects included through the Breit-Pauli Hamiltonian [9]. Another method for solving the electronic-structure problem for divalent atoms relies on the model-potential approximation, see e.g., Ref. [10]. In this method the one-electron eigenvalue problem for a singly charged alkaline-earth ion with a single valence electron is solved first. Using the solutions of the one-electron problem, one constructs two-electron basis functions and an effective two-electron Hamiltonian, which fully incorporates valence-electron correlation. In this way, the eigenenergies and eigenvectors of the two-electron valence shell can be obtained. One more approach (used in this paper) is to employ a systematic formalism that combines advantages of methods of configuration interaction and many-body perturbation theory (CI+MBPT method). Relativistic effects are included exactly, as the formalism starts from the Dirac Hamiltonian and employs relativistic bi-spinor wave functions. A resulting theoretical accuracy of the CI+MBPT does not exceed a few percent even for such a relatively-complex atom as ytterbium.

## A. CI+MBPT method

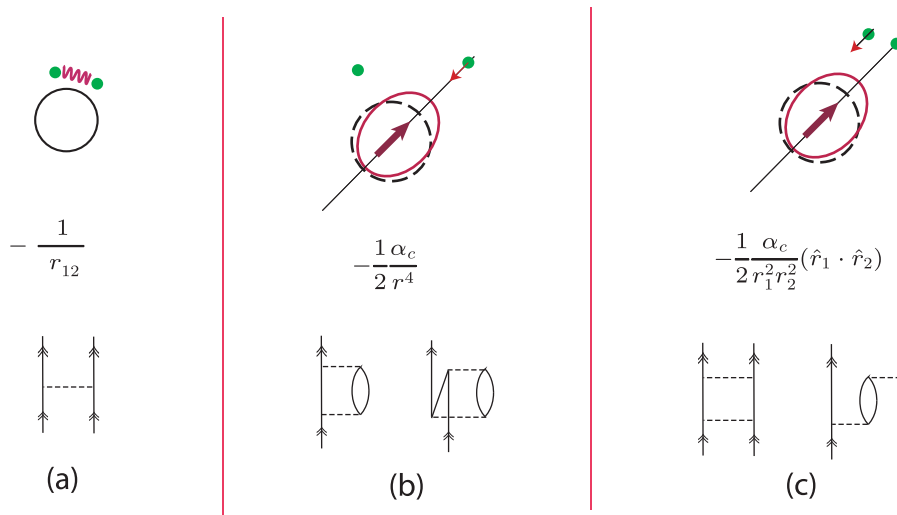


FIG. 2: Major correlation effects for the divalent atoms. Panel (a): strong repulsion between the two-valence electrons. Panel (b): self-induced (or self-energy) core-polarization attraction. Panel (c) cross-induced (or screening) core-polarization effect. We depict two valence electrons as dots above the closed shell core. Polarization of the core by the electrons is shown as deformation of the core with the heavy arrow showing the direction of the polarization. The induced dipole field causes attraction of either perturbing (panel (b)) or the spectator (panel (c)) electron. The formulas below the sketches represent an approximation characteristic of model-potential treatments,  $\alpha_c$  being core polarizability and  $r_1$  and  $r_2$  being coordinates of the valence electrons. Their many-body analogs are represented by the lowest-order (panel (a)) and second-order (panels (b) and (c)) Brueckner-Goldstone diagrams.

Many-body perturbation theory (MBPT) provides a systematic prescription for solving the atomic many-body problem [11]. Basically, the interaction between the electrons is treated as a perturbation and one applies the machinery similar to the textbook stationary perturbation theory. The MBPT produces excellent results for alkali-metal atoms which have only one electron outside closed shells. Even for atoms as heavy as Cs (55 electrons), the modern *ab initio* many-body relativistic techniques demonstrate an accuracy of 0.1% for energy levels, and a few 0.1% for hyperfine structure constants and lifetimes [12].

One could easily see that bringing the MBPT techniques from univalent to divalent atoms requires substantial revision of the methods. Indeed let us consider calculations for the ground state of Be atom ( $1s^2 2s^2$  configuration). If we start our perturbative treatment from the Coulomb wave functions, the  $2s$  and  $2p$  orbitals have the same energies and because of the degeneracy, we immediately acquire infinitely large terms in the perturbative expansion. Even if we start our analysis from the more accurate Hartree-Fock approximation, the levels remain nearly degenerate and the perturbative treatment breaks down.

These near-degenerate cases have to be treated essentially non-perturbatively using the configuration interaction (CI) or multiconfiguration Hartree-Fock methods. The accuracy of the CI is limited only by the completeness of the set of configurations used. For a many-electron atom the number of possible configurations is enormous and one has to select only a small fraction of them (this subspace is usually referred to as the model space). In our treatment the model space is limited to valence excitations. The contributions of remaining configurations (i.e., the ones involving excitations of core electrons) are treated within the MBPT. The convergence of the perturbative expansion involving the core-excited states is sufficiently rapid, reflecting relatively large energy denominators.

To summarize, the accuracy of the MBPT and the (restricted) CI methods is limited in different sectors of the many-body problem. MBPT is not accurate in describing valence-valence interactions, while the CI fails to fully account for the core-valence and core-core correlations. For this reason it is natural to combine the two methods in an attempt to reach higher accuracy for multi-valent atoms. A general treatment of the correlation problem along these lines can be found, e.g., in the monograph on atomic MBPT [11]. In our case we employ the method combining the configuration interaction and the many-body perturbation theory as implemented by Dzuba, Kozlov, and Flambaum [13]. It was initially used for accurate calculations of low-lying energy levels of atoms and then extended to calculations of various observables such as hyperfine structure constants, oscillator strengths, lifetimes, polarizabilities, and parity non-conserving amplitudes [14–21]. In the following we refer to this method as the CI+MBPT method.

TABLE II: Two-electron binding energies in a.u. and energy differences in  $\text{cm}^{-1}$  for low-lying levels of Sr [20].

Config.	Level	CI		CI+MBPT		Experiment [22]	
		$E_{\text{val}}$	$\Delta$	$E_{\text{val}}$	$\Delta$	$E_{\text{val}}$	$\Delta$
$5s^2$	$^1S_0$	0.586538	—	0.614409 <sup>a</sup>	—	0.614601 <sup>b</sup>	—
$5s\ 4d$	$^3D_1$	0.497148	19619	0.532110	18063	0.531862	18159.1
$5s\ 4d$	$^3D_2$	0.497077	19635	0.531809	18129	0.531590	18218.8
$5s\ 4d$	$^3D_3$	0.496941	19664	0.531298	18242	0.531132	18319.3
$5s\ 4d$	$^1D_2$	0.494339	20235	0.522311	20213	0.522792	20149.7
$5s\ 6s$	$^3S_1$	0.460940	27566	0.481533	29162	0.482291	29038.8
$5s\ 5p$	$^3P_0^o$	0.529636	12489	0.548754	14410	0.549366	14317.5
$5s\ 5p$	$^3P_1^o$	0.528850	12662	0.547896	14598	0.548514	14504.4
$5s\ 5p$	$^3P_2^o$	0.527213	13021	0.546079	14997	0.546718	14898.6
$5s\ 5p$	$^1P_1^o$	0.491616	20833	0.515901	21621	0.515736	21698.5

<sup>a</sup> This value obtained with  $\delta = -0.3$  a.u. <sup>b</sup>For the ground state  $E_{\text{val}} = \text{IP}(\text{Sr}) + \text{IP}(\text{Sr}^+)$ , where ionization potential (IP) for Sr =  $45925.6\ \text{cm}^{-1}$  and IP ( $\text{Sr}^+$ ) =  $88964.0\ \text{cm}^{-1}$  [22].

A detailed description of the CI+MBPT method can be found in papers [13–21]. Here we only briefly recapitulate its main features. We consider Mg, Ca, Sr and Yb as atoms with two valence electrons outside the closed-shell core. The strong repulsion between the two valence electrons is treated non-perturbatively using the configuration-interaction method. The core-valence and core-core correlations are taken into account with the help of the many-body perturbation theory method.

The atomic spectrum is found from the equation for the valence electrons:

$$H_{\text{eff}}(E_n)|\Psi_n\rangle = E_n|\Psi_n\rangle, \quad (1)$$

where the effective Hamiltonian consists of two parts

$$H_{\text{eff}}(E) = H_{\text{FC}} + \Sigma(E).$$

Here  $H_{\text{FC}}$  is the Hamiltonian in the frozen core approximation and  $\Sigma$  is the energy-dependent correction, which takes into account virtual core excitations. Representative diagrams entering the operator  $\Sigma$  are shown in panels (b) and (c) of Fig.2. It is worth emphasizing that the underlying calculations are *ab initio* relativistic and are based on the Dirac equation and involve relativistic bi-spinors with large and small components of the electronic wave function.

At this stage we are able to fully account for the second order of the perturbation theory and partially for the high-order corrections of the MBPT. The latter requires special discussion. The second order corrections to the Hamiltonian include both the one-electron (self-energy diagrams in panel (b) of Fig.2) and the two-electron ones (see the screening diagrams in panel (c) of Fig.2). This latter are specific for atoms with several valence electrons. A number of the two-electron diagrams is very large and their calculation is extremely time-consuming. In the higher orders the calculation of two-electron diagrams becomes impractical. Respectively, it is more promising to account for the high-orders of the MBPT indirectly. One of such methods was suggested in Ref. [16], where it was shown that a proper choice of the optimum initial approximation for the effective Hamiltonian can substantially improve the agreement between calculated and experimental spectra of a multielectron atom. One introduces an energy shift  $\delta$  and makes the replacement  $\Sigma(E) \longrightarrow \Sigma(E - \delta)$ . This leads to the equation

$$H_{\text{eff}}(E_n - \delta)|\Psi_n\rangle = E_n|\Psi_n\rangle.$$

By solving this equation with different  $\delta$ , we obtain  $E_n(\delta)$ . If we choose  $\delta=0$ , we have the Brillouin-Wigner variant of the MBPT. Other choices of  $\delta$  can give us different variants of the perturbation theory. In particular, the Rayleigh-Schrödinger variant of the MBPT corresponds to  $\delta = E_n - E_n^{(0)}$ , where  $E_n^{(0)}$  is the zero order energy of the level  $n$ . For few electron systems an intermediate value of  $\delta$  is optimal. This value can be found by fitting of energy levels.

As an example we present in Table II numerical results for the low-lying energy levels of atomic Sr. The results are given for the cases of the pure CI and the CI+MBPT. As is seen from the table the two-electron binding energies are reproduced very well. Already at the CI stage the agreement of the calculated and experimental energies is on the level of 5%. Account for the MBPT corrections allows us to improve the accuracy by approximately an order of magnitude and the use of the optimal  $\delta$  gives the final accuracy of  $\sim 0.1$ - $0.2\%$ .

After the optimized effective Hamiltonian is constructed and wave functions of the ground and the low-lying excited states are found they can be used for calculations of other atomic quantities such as hyperfine structure constants,  $E1$  transition amplitudes, and polarizabilities. For calculation of the matrix elements we apply the technique of effective

TABLE III: Magnetic-dipole hyperfine structure constants  $A$  for the  $nsnp\ ^3P_1$  and  $nsnp\ ^3P_2$  states. The computed CI+MBPT values [24] are compared with the experimental data.

		$A(^3P_1)$ (MHz)	$A(^3P_2)$ (MHz)
$^{25}\text{Mg}$	CI+MBPT	-146.1	-129.7
	Experiment	-144.977(5) <sup>a</sup>	-128.445(5) <sup>a</sup>
$^{43}\text{Ca}$	CI+MBPT	-199.2	-173.1
	Experiment	-198.890(1) <sup>b</sup>	-171.962(2) <sup>c</sup>
$^{87}\text{Sr}$	CI+MBPT	-258.7	-211.4
	Experiment	-260.083(5) <sup>d</sup>	-212.765(1) <sup>d</sup>
$^{171}\text{Yb}$	CI+MBPT	3964	2704
	Experiment	3957.97(47) <sup>e</sup>	2677.6 <sup>f</sup>
$^{173}\text{Yb}$	CI+MBPT	-1092	-745
	Experiment	-1094.20(60) <sup>e</sup>	-737.7 <sup>f</sup>

<sup>a</sup> Lurio [25], <sup>b</sup> Arnold et al. [26], <sup>c</sup> Grundevik et al. [27], <sup>d</sup> Heider and Brink [28], <sup>e</sup> Clark et al. [29], <sup>f</sup> Budick and Snir [30].

TABLE IV: Reduced matrix elements for transitions from the low-lying  $nsnp\ ^3,^1P_1^o$  states to the ground  $ns^2\ ^1S_0$  state are presented in a.u. The computed values are compared to the values known from the experiments.

	$ \langle ns^2\ ^1S_0    D    nsnp\ ^3P_1 \rangle $		$ \langle ns^2\ ^1S_0    D    nsnp\ ^1P_1 \rangle $	
	CI+MBPT	Experiment	CI+MBPT	Experiment
Mg	0.0064(7) <sup>a</sup>	0.0053(3) <sup>b</sup> 0.0056(4) <sup>d</sup>	4.03(2) <sup>a</sup>	4.12(6) <sup>c</sup> 4.06(10) <sup>e</sup>
Ca	0.034(4) <sup>a</sup>	0.0357(4) <sup>f</sup> 0.0352(10) <sup>h</sup>	4.91(7) <sup>a</sup>	4.905(22) <sup>g</sup>
Sr	0.160(15) <sup>a</sup>	0.1555(16) <sup>i</sup>	5.28(9) <sup>a</sup>	5.249(2) <sup>j</sup>
Yb	0.54(8) <sup>k</sup>	0.549(4) <sup>l</sup>	4.4(8) <sup>k</sup>	4.148(2) <sup>m</sup>

<sup>a</sup> Porsev et al. [20], <sup>b</sup> Godone and Novero [31], <sup>c</sup> Smith and Gallagher [32], <sup>d</sup> Kwong et al. [33], <sup>e</sup> Lundin et al. [34], <sup>f</sup> Husain and Roberts [35], <sup>g</sup> Degenhardt et al. [36], <sup>h</sup> Drozdowski et al. [37], <sup>i</sup> Husain and Schifino [38], <sup>j</sup> Yasuda et al. [39], <sup>k</sup> Porsev et al. [18], <sup>l</sup> Bowers et al. [40], <sup>m</sup> Takasu et al. [41].

all-order (“dressed”) operators. Technically, we employ the random-phase approximation (RPA). The RPA sequence of diagrams describes a shielding of externally applied field by the core electrons. We additionally incorporate smaller corrections: Brueckner corrections to core orbitals, subtraction and two-particle corrections, correction to structural radiation and normalization. The detailed discussion of these corrections can be found elsewhere [21]. Note that the most-important contributions to matrix elements are associated with the RPA corrections.

To demonstrate the quality of the constructed wave functions and the accuracy of the effective-operator approach, we present in Tables III and IV the calculated magnetic-dipole hyperfine structure constants  $A$  for the  $^3P_{1,2}$  states and the reduced matrix elements  $\langle ns^2\ ^1S_0 || D || nsnp\ ^3,^1P_1 \rangle$  of electric dipole operator  $D$  for the transitions from the low-lying odd-parity  $^3,^1P_1$  states to the ground state [20]. As seen from Table III the differences between the calculated and the experimental values for the constants  $A$ , even for heavy Yb, do not exceed 1%. For the heaviest and more computationally demanding Yb, the corrections to the effective hyperfine operator tend to cancel [17], and we have simplified the calculations for Yb by omitting “dressing” and using the bare hyperfine operator.

The results presented in Table IV demonstrate the increasing importance of correlations when progressing from lighter to heavier atoms. For heavier atoms the MBPT corrections to the matrix elements grow larger and as a result the accuracy of calculations becomes worse. For example, for the  $\langle ns^2\ ^1S_0 || D || nsnp\ ^1P_1 \rangle$  electric-dipole matrix element the accuracy of the CI+MBPT method is 0.5% for Mg but only 18% for Yb. This is hardly surprising because we fully account for only the second order of the perturbation theory. For heavy atoms the higher orders of the MBPT play a significant role. In Ref. [23] a similar relativistic approach was used for calculating  $E1$  transition amplitudes for divalent atoms and the obtained results are in a fair agreement with our results [20].

## B. Sternheimer-Dalgarno-Lewis method

A usual problem encountered in evaluating atomic properties relevant to lattice clocks is a computation of second-order sums over a complete set of atomic many-body states. One of such properties is the dynamic polarizability of atomic states entering Stark shift of the levels in the laser field. The problem of determining the complete set of states

needed for summations becomes quickly impractical for divalent atoms. It is more convenient to lump contributions of the intermediate states into a single “perturbed” state. This method is conventionally referred to as the Sternheimer-Dalgarno-Lewis method [42, 43]). Below we recapitulate the main features of this method, its implementation in the CI+MBPT framework, and illustrate the technique by computing static polarizabilities of divalent atoms. The presented static polarizabilities are relevant to evaluating black-body radiation shifts, see Sec. VII.

We would like to evaluate a second-order sum  $\mathcal{F}$  that depends on matrix elements of operators  $\mathcal{A}$  and  $\mathcal{B}$ ,

$$\mathcal{F} = \sum_k \frac{\langle \Psi_0 | \mathcal{A} | \Psi_k \rangle \langle \Psi_k | \mathcal{B} | \Psi_0 \rangle}{E_k - E_0}. \quad (2)$$

States  $\Psi_k$  are the eigenfunctions of atomic Hamiltonian,  $H$ , with energies  $E_k$ . Instead of direct summation over the intermediate states one can find an intermediate-state “lumped” wave function  $|\delta\Psi\rangle$  from an inhomogeneous equation

$$(H - E_0)|\delta\Psi\rangle = \sum_k |\Psi_k\rangle \langle \Psi_k | \mathcal{B} | \Psi_0 \rangle = \mathcal{B}|\Psi_0\rangle. \quad (3)$$

With the computed  $|\delta\Psi\rangle$ , the quantity of interest, Eq. (2), is obtained simply as

$$\mathcal{F} = \langle \Psi_0 | \mathcal{A} | \delta\Psi \rangle. \quad (4)$$

This approach is generalized in a straightforward way to higher orders of the perturbation theory, i.e., when Eq. (2) includes more than two operators and several summations over intermediate states.

To illustrate an implementation of the Sternheimer-Dalgarno-Lewis method in the CI+MBPT framework we present in Table V the results of computing the static scalar electric-dipole polarizabilities of the  $ns^2\ ^1S_0$  and  $nsnp\ ^3P_0$  clock states which are needed, for instance, for evaluating black-body radiation shifts, see Sec. VII. The details of calculations can be found in [44]. Here we only briefly describe the main points. In the frame of the CI+MBPT method all electrons are separated into two groups: valence and core electrons. The intermediate states in Eq. (2) can be separated accordingly into valence-excited states and core-excited states. The first group of states is obtained by promoting valence electrons to other valence shells. As a result the intermediate state remains in the model (CI) space of the effective Hamiltonian Eq. (1). The second group of states may, in addition, involve real excitations of the core electrons. These excitations necessarily live in the space complementary to the model space.

If an initial state  $|\Psi_0\rangle$  is the state with the total angular momentum  $J = 0$  the static scalar electric dipole polarizability of a state  $|\Psi_0\rangle$  is defined as

$$\alpha_0^{(E1)}(0) = 2 \sum_k \frac{\langle \Psi_0 | D_0 | \Psi_k \rangle \langle \Psi_k | D_0 | \Psi_0 \rangle}{E_k - E_0}. \quad (5)$$

Apparently the polarizabilities can be computed with the help of Eqs. (2-4) with  $\mathcal{A} = \mathcal{B} \equiv D_0$ , where  $D_0$  is the z-component of the operator of the electric dipole moment. For brevity in this subsection we denote  $\alpha \equiv \alpha_0^{(E1)}(0)$ .

Following the approach suggested in [45] and briefly discussed above we decompose the polarizability, Eq. (5), into three parts

$$\alpha = \alpha_v + \alpha_c + \alpha_{cv}. \quad (6)$$

Here  $\alpha_v$  is a traditional term encapsulating excitations of the valence electrons. This part gives dominant contribution to the polarizability. Once the wave functions of the valence electrons  $|\Psi_0\rangle$  are found from the eigenvalue equation, Eq. (1), the valence polarizabilities  $\alpha_v$  are computed with the formally exact Sternheimer-Dalgarno-Lewis method implemented in the CI+MBPT framework. From Eq. (3) we find

$$\begin{aligned} |\delta\Psi\rangle &= \frac{1}{H_{\text{eff}} - E_0} \sum_k |\Psi_k\rangle \langle \Psi_k | D_0 | \Psi_0 \rangle \\ &= \frac{1}{H_{\text{eff}} - E_0} D_0 |\Psi_0\rangle, \end{aligned} \quad (7)$$

and finally obtain for the valence part of the polarizability

$$\alpha_v = 2 \langle \Psi_0 | D_0 | \delta\Psi \rangle. \quad (8)$$

TABLE V: Static electric dipole polarizabilities in a.u. for the ground  $^1S_0$  and the lowest-energy  $^3P_0$  excited states of Mg, Ca, Sr, and Yb atoms [44]. Theoretical uncertainties are indicated in parentheses.

	Mg	Ca	Sr	Yb
$\alpha_{^1S_0}$	71.3(7)	157.1(1.3)	197.2(2)	120.5(3.1)
$\alpha_{^3P_0}$	101.2(3)	290.3(1.5)	458.3(3.6)	266(15)

Contribution of core-excited states to the polarizability denoted by  $\alpha_c$  has to be added separately. Here we follow the work [45] and use the relativistic random-phase approximation [46] to determine the core polarizability as

$$\alpha_c = \sum_{\omega_\mu > 0} \frac{f_\mu}{\omega_\mu^2}, \quad (9)$$

where the summation is over particle-hole excitations from the ground state of the atomic core;  $\omega_\mu$  are excitation energies and  $f_\mu$  are the corresponding electric-dipole oscillator strengths. Accounting for core excitations is essential in our accurate calculations, especially for heavier atoms. Finally, a small counter term  $\alpha_{cv}$  is related to excitations of core electrons to occupied valence states. Because we include the Pauli-principle-forbidden excitations in the calculations of core polarizabilities, we have to introduce the counter term.

Table V summarizes our numerical results for the static scalar electric polarizabilities. First we discuss the results for the ground-state polarizabilities. Values for Mg, Ca, and Sr were obtained in Ref. [47] and for Yb in Ref. [44]. To estimate their uncertainties we use the fact that the intermediate state  $nsnp\ ^1P_1$  contributes to the polarizability at the level of 95-97%. Taking this into account we can single out the contribution to (5) that characterizes the E1 transition from the ground state to the lowest-lying  $nsnp\ ^1P_1$  state and makes the major contribution to the electric dipole polarizability of the ground state  $ns^2\ ^1S_0$ . We can then write  $\alpha_v$  as the sum of two terms

$$\alpha_v = \alpha_v^p + \alpha_{v'}, \quad (10)$$

where

$$\alpha_v^p \equiv 2 \frac{|\langle nsnp\ ^1P_1 | D_0 | ns^2\ ^1S_0 \rangle|^2}{E_{^1P_1} - E_{^1S_0}}, \quad (11)$$

and  $\alpha_{v'}$  includes all the other terms of the sum over  $k$  in Eq. (5).

For calculating the polarizabilities the best-known literature values of the reduced matrix elements  $\langle ns^2\ ^1S_0 || D || nsnp\ ^1P_1 \rangle$  tabulated in [47] were used. For instance, for Sr it was obtained from a high precision measurement of the lifetime of the  $5s5p\ ^1P_1$  state [39]:  $|\langle 5s^2\ ^1S_0 || D || 5s5p\ ^1P_1 \rangle| = 5.249(2)$  a.u. leading to the 0.1% uncertainty in  $\alpha_v(^1S_0)$ . Contribution of the core corrections to the polarizability for this case ( $\alpha_c + \alpha_{cv} = 5.4$  a.u. [47]) is less than 3%. Because the uncertainty of the latter can be roughly estimated as 1% [48] the final uncertainty of the polarizability  $\alpha$  is at the level of 0.1%. The uncertainties in the remaining polarizabilities were estimated as one half of the difference between two predictions obtained with  $\delta = 0$  and with  $\delta$  determined with the best fit to the experimental energies (thus mimicking omitted higher-order many-body corrections). The uncertainties in the ground-state polarizabilities range from 0.1% for Sr to 3% for Yb.

For the  $^3P_0$  states the uncertainties range from 0.3% for Mg to 6% for Yb. Unlike in the case of the ground state, the polarizability of the  $^3P_0$  states is accumulated due to several transitions: the lowest-energy  $^3D_1$  states contribute only at the level of 50-60%. In Mg the contribution of the  $3s4s\ ^3S_1$  state is even larger than the contribution of the  $3s3d\ ^3D_1$  state. Generally, the accuracy of the calculations becomes worse for heavier atoms. This follows the general trend of many-body calculations, where the correlations, and thus the omitted higher orders of perturbation theory, become increasingly important as the number of electrons grows. The results presented in Table V for the ground states of divalent atoms are in good agreement with other calculations (see, e.g., [49, 50]) and with experimental results [34, 36, 51]. Unfortunately, the existing experiments are not sufficiently accurate to test our predictions.

In this section we briefly described the main features of the CI+MBPT method that couples the configuration interaction technique with the many-body perturbation theory. We presented the results of calculations of different quantities (energies of the low-lying levels for Sr, hyperfine structure constants and E1 transition amplitudes for divalent atoms) in the CI+MBPT framework. We also discussed evaluation of sums over a complete set of intermediate states using the Sternheimer-Dalgarno-Lewis method and random-phase approximation. We illustrated our technique by evaluating the static scalar electric-dipole polarizabilities of the clock states for Mg, Ca, Sr, and Yb. In general, we find that the CI+MBPT approach is capable of reliably and accurately predicting a wide variety experimental observables, ranging from hyperfine constants to lifetimes and energies.

### III. MAGIC WAVELENGTH

In the following Sections, we evaluate lattice clock-related parameters. In the lattice clocks, the atoms are confined to sites of an optical lattice (formed by a standing-wave laser field). We start off with analyzing a quantity central to the Stark-free spectroscopy, the selection of the wavelength of the lattice laser. At a certain, “magic”, value of the wavelength, the laser-induced perturbations of both clock levels are identical and the atom responds spectroscopically as if it were placed in an artificial vacuum. The determination of the magic wavelength does not, fortunately, require magic: it involves computation of dynamic polarizabilities. While usually knowing the dominant electric-dipole polarizability is sufficient, the higher-multipole (e.g., magnetic-dipole, electric-quadrupole, . . .) polarizabilities may introduce additional corrections to the Stark shifts and affect values of the magic wavelength. Therefore, based on the Floquet approach and multipolar expansions we derive in this Section the general multipolar dynamic polarizabilities. Further we illustrate the derived expressions by numerically determining the magic wavelength for ytterbium clock.

#### A. Second-order dynamic response

In this section first we review the formalism of quasi-energy states (Floquet formalism) and then apply it to deriving atomic properties relevant to the design of lattice clock. The Floquet formalism, as it applies to the atom-laser interaction was reviewed, for example, by Manakov *et al.* [52]. One considers an interaction of a quantum system with a monochromatic perturbation

$$V(t) = v^{(-)}e^{-i\omega t} + v^{(+)}e^{+i\omega t}. \quad (12)$$

This perturbation drives a system characterized by the time-independent Hamiltonian  $H_0$  and the “bare” eigenspectrum  $\{\psi_a, E_a\}$ , so that

$$H_0\psi_a = E_a\psi_a.$$

In the Floquet formalism, the entire Hamiltonian is replaced by

$$H \rightarrow H - i\frac{\partial}{\partial t},$$

and the inner product is extended to include the time-averaging over the period of the perturbation  $T = 2\pi/\omega$ ,

$$\langle\langle\phi_i|\phi_k\rangle\rangle = \frac{1}{T} \int_0^T \langle\phi_i|\phi_k\rangle dt, \quad (13)$$

$\langle\phi_i|\phi_k\rangle$  being the traditional inner product. In the lowest order we deal with the “dressed” atomic states

$$\phi_{a,k} = \psi_a e^{ik\omega t}, \quad k = 0, \pm 1, \pm 2, \dots \quad (14)$$

$$E_{a,k} = E_a + k\omega, \quad (15)$$

where the functions  $\phi_{a,k}$  satisfy the modified Schrodinger equation

$$\left(H_0 - i\frac{\partial}{\partial t}\right) \phi_{a,k} = E_{a,k}\phi_{a,k}.$$

Since the time-derivative is already incorporated in the formalism, one may show that the expressions from the stationary perturbation theory may be employed to describe the response to the monochromatic  $V(t)$ . In the “upgraded” expressions all the “bare” eigenfunctions and energies are replaced by their “dressed” counterparts and the inner products are extended according to the prescription (13). For example, the lowest-order correction reads

$$E_a^{(1)} = \langle\langle\phi_{a,0}|V|\phi_{a,0}\rangle\rangle.$$

This correction vanishes for the electric-dipole interactions and the atomic states of definite parity, and the second-order expression will be of particular interest to us

$$E_a^{(2)} = \sum_{b,k} \frac{\langle\langle\phi_{a,0}|V|\phi_{b,k}\rangle\rangle\langle\langle\phi_{b,k}|V|\phi_{a,0}\rangle\rangle}{E_a - E_{b,k}}.$$

Explicit evaluation of the extended inner products limits the sums to single-photon transitions ( $k = \pm 1$ ) leading to the familiar result

$$E_a^{(2)} = \sum_b \frac{|\langle \psi_a | v^{(+)} | \psi_b \rangle|^2}{E_a - (E_b - \omega)} + \sum_b \frac{|\langle \psi_a | v^{(-)} | \psi_b \rangle|^2}{E_a - (E_b + \omega)}. \quad (16)$$

While the above second-order result can be recovered in the more traditional secular approximation (see, e.g., Sec. VII) of the time-dependent perturbation theory, the advantage of the Floquet formalism is that one could employ the higher-order expressions from the less complicated time-*independent* perturbation theory and readily derive corresponding high-order corrections (such as hyperpolarizability) to the energy shift in the oscillating fields. We will employ this technique for deriving hyperfine-induced light shifts in Sec. V.

As a familiar example, consider a perturbation by a linearly polarized electric field

$$V(t) \equiv V_{E1}(t) = -D_z \mathcal{E}_0 \cos \omega t = -\frac{1}{2} D_z \mathcal{E}_0 (e^{i\omega t} + e^{-i\omega t}),$$

where  $D_z$  is the component of the atomic electric dipole moment along the electric field. By comparing with Eq.(12) we identify  $v^{(+)} = v^{(-)} = -D_z \mathcal{E}_0 / 2$ , and from Eq.(16) we immediately recover the well-known result

$$E_a^{(2)} = -\frac{1}{4} \mathcal{E}_0^2 \alpha_a^{E1}(\omega), \quad (17)$$

$$\alpha_a^{E1}(\omega) = 2 \sum_b \frac{E_b - E_a}{(E_b - E_a)^2 - \omega^2} |\langle \psi_a | D_z | \psi_b \rangle|^2, \quad (18)$$

with  $\alpha_a^{E1}(\omega)$  being the dynamic (a.c.) electric-dipole polarizability of the state  $a$ .

## B. Dynamic multipolar polarizabilities

Here we apply the Floquet formalism to derive the expressions for the dynamic multipolar polarizabilities. We use the relativistic approach. Incidentally, compared to the nonrelativistic treatment, the relativistic formulation leads to more concise derivations, as the couplings are linear in the vector potential. An interaction of an electron with the EM field reads (to unclutter notation, here we consider only a single electron, the generalization for the many-electron case being straightforward)

$$V = \boldsymbol{\alpha} \cdot \mathbf{A}(\mathbf{r}, t) - \Phi(\mathbf{r}, t),$$

where  $A$  and  $\Phi$  are the magnetic and electric potentials, respectively and  $\boldsymbol{\alpha}$  represents a collection of the conventionally defined Dirac matrices [53]. For an electromagnetic wave in the transverse gauge (where  $\Phi \equiv 0$ ), the perturbation reduces to  $V = (\boldsymbol{\alpha} \cdot \mathbf{A})$  with the vector potential

$$\mathbf{A} = \frac{1}{2} \hat{\boldsymbol{\varepsilon}} A_0 e^{i(\mathbf{k} \cdot \mathbf{r})} e^{-i\omega t} + c.c.,$$

where  $\hat{\boldsymbol{\varepsilon}}$  is the polarization vector (this may include circular and linear polarizations) and *c.c.* stands for the complex conjugate. The amplitude  $A_0$  is related to the laser intensity  $I$  as  $I = \frac{\omega^2}{8\pi c} |A_0|^2$  and the corresponding amplitude of the electric field  $\mathcal{E}_0 = A_0 \omega / c$ . The wavevector  $k = \omega / c = \alpha \omega$  in atomic units. We identify,

$$v^{(-)} = \frac{1}{2} A_0 (\boldsymbol{\alpha} \cdot \hat{\boldsymbol{\varepsilon}}) e^{i(\mathbf{k} \cdot \mathbf{r})}, \quad v^{(+)} = \frac{1}{2} A_0 (\boldsymbol{\alpha} \cdot \hat{\boldsymbol{\varepsilon}}^*) e^{-i(\mathbf{k} \cdot \mathbf{r})}.$$

### 1. Multipolar expansion

At this point we focus on multipolar fields. We will use the outlined multipolar formalism in this Section and later in Section VII. The reader is referred to Ref. [54, 55] for additional details.

We make use of the multipolar expansion of  $\boldsymbol{\varepsilon} e^{i(\mathbf{k} \cdot \mathbf{r})}$  in vector spherical harmonics  $\mathbf{Y}_{JM}^{(\lambda)}$  [56]

$$\boldsymbol{\varepsilon} e^{i(\mathbf{k} \cdot \mathbf{r})} = 4\pi \sum_{JM\lambda} i^{J-\lambda} \left( \mathbf{Y}_{JM}^{(\lambda)}(\hat{\mathbf{k}}) \cdot \hat{\boldsymbol{\varepsilon}} \right) \mathbf{a}_{JM}^{(\lambda)}(\mathbf{r}), \quad (19)$$

where  $\lambda = 0$  is for magnetic (MJ) and  $\lambda = 1$  is for electric (EJ)  $2^J$ -polar amplitudes. Explicit expressions for the expansion amplitudes  $\mathbf{a}_{JM}^{(\lambda)}(\mathbf{r})$  in terms of the spherical Bessel functions can be found in Ref. [55]; since no expansion is made in powers of  $\mathbf{k} \cdot \mathbf{r}$ , the retardation is built in into the formalism from the onset. We may introduce a similar multipolar expansion for the coupling

$$t(\omega, r) = (\boldsymbol{\alpha} \cdot \hat{\boldsymbol{\varepsilon}}) e^{i\mathbf{k} \cdot \mathbf{r}} = 4\pi \sum_{JM\lambda} i^{J-\lambda} \left( \mathbf{Y}_{JM}^{(\lambda)}(\hat{\mathbf{k}}) \cdot \hat{\boldsymbol{\varepsilon}} \right) \tau_M^{(J\lambda)}, \quad (20)$$

where the tensors  $\tau_M^{(J\lambda)} = \left( \boldsymbol{\alpha} \cdot \mathbf{a}_{JM}^{(\lambda)}(\mathbf{r}) \right)$ .

The irreducible tensor operators  $\tau_M^{(J\lambda)}$  of rank  $J$  may be related to the conventional multipolar operators  $q_M^{(J\lambda)}$  as

$$\tau_M^{(J\lambda)} = i(-1)^{\lambda+1} \left( \frac{(2J+1)(J+1)}{4\pi J} \right)^{1/2} \frac{k^J}{(2J+1)!!} q_M^{(J\lambda)}.$$

Relativistic expressions with retardation for matrix elements of  $q_M^{(J\lambda)}$  can be found in Ref. [55]. Neglecting retardation effects  $q_M^{(J1)}$  become the conventional frequency-independent EJ moments (in the length gauge)

$$q_M^{(J1)} \approx r^J C_{JM}(\hat{\mathbf{r}}),$$

where  $C_{JM}(\hat{\mathbf{r}})$  are the normalized spherical harmonics. In the case of magnetic-dipole transitions in the nonrelativistic limit

$$q_M^{(1,0)} \approx -\frac{\alpha}{2} (\mathbf{L} + 2\mathbf{S})_M.$$

This expression is essentially the nonrelativistic atomic magnetic moment  $\boldsymbol{\mu} = -\mu_B(\mathbf{L} + 2\mathbf{S})$ , with the Bohr magneton  $\mu_B = |e|\hbar/(2m_e c)$  expressed in the Gaussian/atomic units. Further, the retardation brings correction in the order of  $(\alpha\omega)^2$  to these expressions and it may be safely discarded for transitions between low-lying states of neutral systems. For example, neglecting retardation, for the E1 tensor

$$\tau_M^{(1,1)} \approx i \frac{k}{\sqrt{6\pi}} D_M,$$

where  $D_M \equiv q_M^{(1,1)}$  are the spherical components of the traditional electric-dipole operator.

Now we turn our attention to the effect of the multipolar fields on the second-order shift of the atomic energy level

$$E_a^{(2)} = \frac{1}{4} A_0^2 \left\{ \sum_b \frac{|\langle \psi_b | t(\omega, r) | \psi_a \rangle|^2}{E_a - (E_b - \omega)} + \sum_b \frac{|\langle \psi_a | t(\omega, r) | \psi_b \rangle|^2}{E_a - (E_b + \omega)} \right\}. \quad (21)$$

The problem can be solved in general, by substituting expansion (20) in the above expression. Because of our particular emphasis on the lattice clocks, we limit our consideration to spherically-symmetric ( $J_a = 0$ ) atoms. Then only the rotationally-invariant (scalar) component is of relevance.

Below we demonstrate that various multipoles contribute to the light-shift (16) incoherently:  $E_a^{(2)}$  may be represented as a sum over individual multipolar contributions. Indeed, a typical summation in Eq.(16) reduces to

$$|\langle \psi_b | t(\omega, r) | \psi_a \rangle|^2 = (4\pi)^2 \sum_{JM\lambda} \frac{1}{(2J+1)} \delta_{Jb} \delta_{MM_b} \left| \mathbf{Y}_{JM}^{(\lambda)}(\hat{\mathbf{k}}) \cdot \hat{\boldsymbol{\varepsilon}} \right|^2 \left| \langle \psi_b | \tau^{(J\lambda)} | \psi_a \rangle \right|^2,$$

where we used the Wigner-Eckart theorem. To simplify this expression further, we choose the  $z$ -axis along the wavevector  $\mathbf{k}$  and fix the linear polarization along the  $x$ -axis ( $\hat{\boldsymbol{\varepsilon}} = \hat{\mathbf{e}}_x$ ). The result for the scalar polarizability would not depend on the polarization direction. Then for  $\lambda = 0, 1$ , we arrive at  $\mathbf{Y}_{JM}^{(\lambda)}(\hat{\mathbf{e}}_z) \cdot \hat{\mathbf{e}}_x = \sqrt{\frac{2J+1}{16\pi}} \left( \delta_{M,-1} + (-1)^\lambda \delta_{M,+1} \right)$ . The final result may be represented as a sum over multipolar a.c. polarizabilities,

$$E_a^{(2)}(J_a = 0) = \frac{\mathcal{E}_0^2}{4} \sum_{J\lambda} \alpha_a^{(J\lambda)}(\omega), \quad (22)$$

each being defined as

$$\alpha_a^{(J\lambda)}(\omega) = \frac{J+1}{J} \frac{k^{2J-2}}{[(2J-1)!!]^2} \sum_b \left\{ \frac{E_a - E_b}{(E_a - E_b)^2 - \omega^2} \right\} \left| \langle \psi_b | q_0^{(J\lambda)} | \psi_a \rangle \right|^2. \quad (23)$$

In the lattice clocks the frequency of the lattice laser is chosen in such a way that the a.c. Stark shifts of the two clock levels are exactly the same (“magic” frequency.) To the leading order the E1 polarizability overwhelms the a.c. Stark shift. Compared to the E1 contribution, the higher-order multipole polarizabilities are suppressed by a factor of  $(\alpha\omega)^{2J-2}$  for EJ and by a factor of  $\alpha^2(\alpha\omega)^{2J-2}$  for MJ multipoles. Nevertheless, the higher-order multipolar a.c. shifts may modify the value of the magic frequency. From the general formula, Eq.(23), we immediately obtain for the magnetic-dipole polarizability,

$$\alpha_a^{(M1)}(\omega) = 2 \sum_b \left\{ \frac{E_a - E_b}{(E_a - E_b)^2 - \omega^2} \right\} \left| \langle \psi_b | q_0^{(1,0)} | \psi_a \rangle \right|^2, \quad (24)$$

and for the electric-quadrupole a.c. polarizability,

$$\alpha_a^{(E2)}(\omega) = \frac{1}{6} (\alpha\omega)^2 \sum_b \left\{ \frac{E_a - E_b}{(E_a - E_b)^2 - \omega^2} \right\} \left| \langle \psi_b | q_0^{(2,1)} | \psi_a \rangle \right|^2. \quad (25)$$

### C. Ytterbium magic wavelength

Now we illustrate the developed formalism by presenting numerical results for Yb lattice clock [3]. First we compute the E1 a.c. polarizabilities, Eq. (18), with the CI+MBPT method, as described in Section II. The results of the calculations for both  $6s^2\ ^1S_0$  and  $6s6p\ ^3P_0$  states are shown in Fig. 3. According to our calculations the two dynamic polarizabilities intersect at the “magic” wavelength  $\lambda^* \approx 752$  nm. This result is in a good agreement with the experimental value 759.25(2) nm obtained recently in [57]. It is worth noting that at  $\omega^*$  the sum (18) for the ground state is dominated by the  $6s6p\ ^1P_1$  state and for the  $6\ ^3P_0$  level by the  $6s7s\ ^3S_1$  state. We estimate that the computed scalar a.c. polarizabilities are a few per cent accurate.

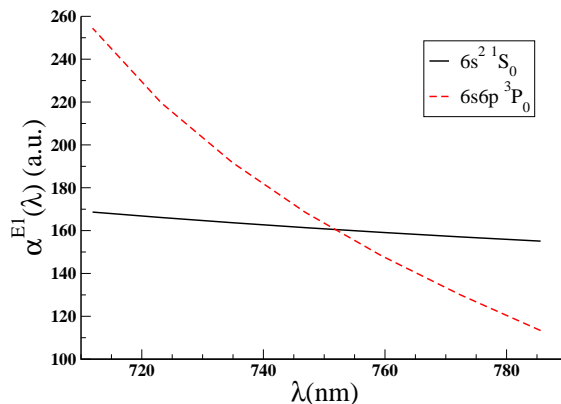


FIG. 3: Electric dipole a.c. polarizabilities for  $6\ ^1S_0$  (solid line) and  $6\ ^3P_0$  (dashed line) states of Yb. The polarizabilities are shown as a function of lattice laser wavelength  $\lambda$ .

We verified that at the magic frequency there are no resonant contributions for the next-order E2 and M1 polarizabilities and we expect  $\alpha^{(E2,M1)} \lesssim 10^{-6} \alpha^{(E1)}$ , similar to the case of Sr [58]. At the same time we notice that a core-excited state  $4f^{13}(^2F_{7/2})5d_{5/2}6s^2\ J = 5$  may become resonant with an excitation from the  $6\ ^3P_0$  level. The relevant  $M5$  polarizability is highly suppressed, and we anticipate that the magic frequency will be only slightly shifted by the presence of this state.

Higher-order correction to the a.c. Stark frequency shift arises due to terms quartic in the field strength  $\mathcal{E}_0$ . This fourth-order contribution is expressed in terms of a.c. hyperpolarizability. The expression for hyperpolarizability [52] has a complicated energy denominator structure exhibiting both single- and two-photon resonances. While for the ground state there are no such resonances, for the  $6\ ^3P_0$  a two-photon resonance may occur for  $6s8p\ ^1P_1$  and  $6s8p\ ^3P_J$

intermediate states. We can not predict if the two-photon resonances would occur, but the experiments [57] indicate that these are not an issue at least presently. For Sr [58] the hyperpolarizability shifts the energy levels by a few mHz at a trapping laser intensity of 10 kW/cm<sup>2</sup>.

#### IV. HYPERFINE QUENCHING OF THE <sup>3</sup>P<sub>0</sub> STATES

The lifetime of the <sup>3</sup>P<sub>0</sub> state determines the natural width of the clock transition between the ground and the <sup>3</sup>P<sub>0</sub> state. For all *bosonic* isotopes of Mg, Ca, Sr, and Yb, the nuclear spin  $I$  vanishes and these isotopes lack hyperfine structure. For bosonic isotopes the <sup>3</sup>P<sub>0</sub> state may decay only via very weak multi-photon transitions. However, for the *fermionic* isotopes,  $I \neq 0$ , a new radiative decay channel becomes available due to the hyperfine interaction (HFI). The HFI admixes  $J = 1$  atomic states opening a fast E1 decay route. The resulting HFI-induced decays determine the lifetimes of the <sup>3</sup>P<sub>0</sub> states and set the natural width of the clock transition.

Below we derive the hyperfine-induced decay rates for fermionic isotopes and compute the decay rates with the accurate CI+MBPT method. We find that the resulting natural widths of the <sup>3</sup>P<sub>0</sub> - <sup>1</sup>S<sub>0</sub> clock transition are 0.44 mHz for <sup>25</sup>Mg, 2.2 mHz for <sup>43</sup>Ca, 7.6 mHz for <sup>87</sup>Sr, 43.5 mHz for <sup>171</sup>Yb, and 38.5 mHz for <sup>173</sup>Yb [24].

##### A. Derivation of hyperfine quenching rates

In the presence of nuclear moments, the total electronic angular momentum  $J$  no longer remains a good quantum number. The atomic energy levels are characterized instead by the total angular momentum  $\mathbf{F} = \mathbf{J} + \mathbf{I}$ . We develop the formalism in terms of the hyperfine states  $|\gamma(IJ)FM_F\rangle$ . Here the angular momenta  $I$  and  $J$  are conventionally coupled to produce a state of definite total momentum  $F$  and its projection  $M_F$ , and  $\gamma$  encapsulates all other atomic quantum numbers. To the lowest order in the hyperfine interaction,  $H_{\text{HFI}}$ , the correction to the hyperfine level  $|\gamma(IJ)FM_F\rangle$  reads

$$|\gamma(IJ)FM_F\rangle^{(1)} = \sum_{\gamma'J'} |\gamma'(IJ')FM_F\rangle \frac{\langle \gamma'(IJ')FM_F | H_{\text{HFI}} | \gamma(IJ)FM_F \rangle}{E(\gamma'J') - E(\gamma J)}, \quad (26)$$

where  $E(\gamma J)$  are the energies of atomic states.

In general, a nucleus may possess a number of magnetic and electric multipole moments. These moments couple to the internal atomic fields and give rise to the hyperfine structure. In this Chapter we are mainly concerned with the properties of the  $J = 0$  states. For all the considered properties, only the magnetic-dipole moment of the nucleus,  $\mu_I$  is relevant (this comes from angular selection rules and more general analysis). The magnetic-dipole hyperfine Hamiltonian,  $H_{\text{HFI}}$ , may be represented by a rotationally-invariant expression

$$H_{\text{HFI}} = (\mathcal{M}^{(1)} \cdot \mathcal{T}^{(1)}). \quad (27)$$

Here  $\mathcal{M}^{(1)}$  is the nuclear magnetic moment operator, with the conventional nuclear moment defined as an expectation value of  $\mathcal{M}^{(1)}$  in the stretched nuclear state

$$\mu_I \equiv \langle IM_I = I | \mathcal{M}_0^{(1)} | IM_I = I \rangle. \quad (28)$$

We list the moments for the isotopes of interest in Table I. The electronic part of the coupling for a point-like nucleus is given by

$$\mathcal{T}_\lambda^{(1)} = i\sqrt{2} \left( \boldsymbol{\alpha} \cdot \mathbf{C}_{1\lambda}^{(0)}(\hat{\mathbf{r}}) \right) / r^2, \quad (29)$$

where  $\mathbf{C}_{1\lambda}^{(0)}(\hat{\mathbf{r}}) = (4\pi/3)^{1/2} \mathbf{Y}_{1\lambda}^{(0)}(\hat{\mathbf{r}})$  is the normalized vector spherical harmonic.

Using the Wigner-Eckart theorem, the matrix element of the hyperfine interaction in Eq. (26) may be simplified to

$$\begin{aligned} \langle \gamma'(IJ'); FM_F | H_{\text{HFI}} | \gamma(IJ); FM_F \rangle &= \delta_{FF'} \delta_{M_F M_F'} \times \\ &(-1)^{I+J'+F} \langle I || \mathcal{M}^{(1)} || I \rangle \langle n'J' || \mathcal{T}^{(1)} || nJ \rangle \left\{ \begin{matrix} I & I & 1 \\ J & J' & F \end{matrix} \right\}. \end{aligned} \quad (30)$$

Now we turn to the derivation of the hyperfine quenching rate. The rate of spontaneous emission for an E1 transition is given by the Fermi golden rule

$$A_{a \rightarrow b} = \frac{4\alpha^3}{3} \omega_{ab}^3 |\langle a | \mathbf{D} | b \rangle|^2, \quad (31)$$

where  $\omega_{ab} = E_a - E_b$  is the transition frequency. Summing over all possible  $F_b$  and magnetic quantum numbers  $M_b$  of the final state, while disregarding small  $F$ -dependent energy correction, one obtains the rate

$$A_{a \rightarrow b} = \frac{4\alpha^3}{3} \omega_{ab}^3 \frac{1}{2F_a + 1} \sum_{F_b} |\langle a || D || b \rangle|^2. \quad (32)$$

For the case at hand, the initial state is the HFI-perturbed  $nsnp\ ^3P_0$  state decaying to the ground  $ns^2\ ^1S_0$  state. Taking into account Eq.(26), we arrive at the hyperfine quenching rate

$$A_{\text{HFI}}(nsnp\ ^3P_0 \rightarrow ns^2\ ^1S_0) = \frac{4\alpha^3}{27} \omega_0^3 \mu_I^2 \frac{I+1}{I} \left| \sum_{\gamma'} \frac{\langle ns^2\ ^1S_0 || D || \gamma' J' \rangle \langle \gamma' J' || \mathcal{T}^{(1)} || nsnp\ ^3P_0 \rangle}{E(\gamma' J') - E(nsnp\ ^3P_0)} \right|^2. \quad (33)$$

Notice that due to the angular selection rules the total electronic angular momentum of the intermediate state is limited to  $J' = 1$ .

## B. Results and conclusions

We carry out numerical evaluation of the HFI-induced rate, Eq.(33) in several logical steps. First, we solve the CI+MBPT eigenvalue problem (see Section II) and determine the ground and the  $nsnp\ ^3P_0$  state wave functions and energies. At the next step, we evaluate the sum over the intermediate states using the Dalgarno-Lewis method, as discussed in Section II B.

The values of the sums over intermediate states grow larger for heavier atoms. This is due to increasing matrix elements of the hyperfine interaction (see Table III). Further, a direct investigation of the sums shows that the contributions of both  $nsnp\ ^3P_1$  and  $nsnp\ ^1P_1$  intermediate states are comparable. Qualitatively, the triplet state is separated from the metastable states by a small fine-structure interval, but its E1 matrix element with the singlet ground state vanishes nonrelativistically. For the singlet state, the situation is reversed: compared to the triplet contribution, the involved energy denominator is much larger, but the electric-dipole matrix element is allowed.

TABLE VI: The hyperfine E1-quenching rates for the metastable  $^3P_0$  states in  $\text{sec}^{-1}$ . The rates are compared with values from the literature. Our CI+MBPT results were previously published in Ref. [24].

Atom	$F$	CI+MBPT	Other
$^{25}\text{Mg}$	5/2	$4.44 \times 10^{-4}$	$4.2 \times 10^{-4}$ <sup>a</sup>
$^{43}\text{Ca}$	7/2	$2.22 \times 10^{-3}$	
$^{87}\text{Sr}$	9/2	$7.58 \times 10^{-3}$	$6.3 \times 10^{-3}$ <sup>b</sup>
$^{171}\text{Yb}$	1/2	$4.35 \times 10^{-2}$	$5.0 \times 10^{-2}$ <sup>c</sup>
$^{173}\text{Yb}$	5/2	$3.85 \times 10^{-2}$	$4.3 \times 10^{-2}$ <sup>c</sup>

<sup>a</sup> Garstang [59], <sup>b</sup> Katori et al. [58], <sup>c</sup> Porsev et al. [3].

In Table VI we present our *ab initio* relativistic CI+MBPT results for the transition rates. Based on a better than 1% accuracy of the *ab initio* hyperfine constants (Table III) and energy levels [17, 20] we expect that the computed hyperfine quenching rate is accurate within at least a few per cent. In Table VI, the CI+MBPT values are also compared with the results from the literature. For Mg the hyperfine quenching rates for the  $^3P_0$  state were estimated more than four decades ago by Garstang [59] (this was motivated by astrophysical applications). Our result is in a reasonable agreement with his values and with previous, less complete, estimates for  $^{87}\text{Sr}$ , Ref. [58], and Yb isotopes [3].

It is worth mentioning one more process that can potentially lead to a shortening of lifetimes of the metastable states. As demonstrated by Yasuda and Katori [60], the blackbody radiation (BBR) induced decay rate of the  $5s5p\ ^3P_2$  state for Sr is equal to  $8.03 \times 10^{-3} \text{ s}^{-1}$  at 300 K. Our order-of-magnitude estimate of the BBR quenching for Mg, Ca, and Yb shows that at room temperature ( $T = 300 \text{ K}$ ) the BBR quenching is negligible compared to the rates caused

by the vacuum fluctuations of the electromagnetic field ( $T = 0$ ). The reader, however, should be cautioned that the BBR rate strongly depends on the ambient temperature and it may become important, for example, if a hot oven is used as a source of atoms.

To summarize the main result of this section, the resulting natural widths of the  $^3P_0 - ^1S_0$  clock transition are 0.44 mHz for  $^{25}\text{Mg}$ , 2.2 mHz for  $^{43}\text{Ca}$ , 7.6 mHz for  $^{87}\text{Sr}$ , 43.5 mHz for  $^{171}\text{Yb}$ , and 38.5 mHz for  $^{173}\text{Yb}$ . These narrow widths translate into the high resonance quality factors characteristic of the lattice-based optical clocks.

## V. HYPERFINE-INDUCED VECTOR LIGHT SHIFT IN THE $^3P_0$ STATE

The second order light shift involves two interactions with the laser field. The product of two interactions ( $D \cdot \mathcal{E})(D \cdot \mathcal{E}^*)$  may be re-coupled into the scalar, vector (axial), and tensor components of the dynamic polarizability. The rotational properties are determined by the respective tensors of rank 0,1, and 2 acting in the electronic space. Because of the angular selection rules, for the  $J = 0$  clock states only the scalar polarizability is of relevance and it was the focus of our discussion in Section III. The hyperfine interaction, nevertheless, removes the spherical symmetry of the atoms and leads to residual vector,  $\alpha_{\gamma F}^A(\omega)$ , and tensor,  $\alpha_{\gamma F}^T(\omega)$  a.c. polarizabilities. These may affect the performance of the clock: vector light shift can cause a small Stark-shift dependence on the polarization of the trapping light.

To determine the effect of the HFI on the a.c. polarizability we carry out an analysis in the third-order perturbation theory. We apply the Floquet formalism (Section III A) with respect to a combined operator

$$V = V_{\text{HFI}} + V_{E1}(t).$$

The third-order energy shift of the atomic energy level reads

$$E_a^{(3)} = \sum_{b,c \neq a} \frac{V_{ab}V_{bc}V_{ca}}{(E_b^{(0)} - E_a^{(0)})(E_c^{(0)} - E_a^{(0)})} - V_{aa} \sum_{b \neq a} \frac{V_{ab}V_{ba}}{(E_b^{(0)} - E_a^{(0)})^2},$$

where matrix elements are evaluated with respect to the dressed basis and inner products involve time-averaging. The relevant terms (involving two E1 laser-atom interactions and one HFI coupling) are

$$\begin{aligned} E_a^{(3)} = & \sum_{b,c \neq a} \frac{(V_{\text{HFI}})_{ab}(V_{E1})_{bc}(V_{E1})_{ca}}{(E_b^{(0)} - E_a^{(0)})(E_c^{(0)} - E_a^{(0)})} + \sum_{b,c \neq a} \frac{(V_{E1})_{ab}(V_{\text{HFI}})_{bc}(V_{E1})_{ca}}{(E_b^{(0)} - E_a^{(0)})(E_c^{(0)} - E_a^{(0)})} + \\ & \sum_{b,c \neq a} \frac{(V_{E1})_{ab}(V_{E1})_{bc}(V_{\text{HFI}})_{ca}}{(E_b^{(0)} - E_a^{(0)})(E_c^{(0)} - E_a^{(0)})} - (V_{\text{HFI}})_{aa} \sum_{b \neq a} \frac{(V_{E1})_{ab}(V_{E1})_{ba}}{(E_b^{(0)} - E_a^{(0)})^2}. \end{aligned}$$

Notice that we work in the dressed atom picture, i.e., the states  $a, b, c$  are products of atomic and photonic states. Also  $(V_{E1})_{aa} = 0$  due to the parity/angular/photon number selection rules leading to a simplification of the last term. Explicitly, after the time averaging, Eq.(13), (now  $a, b, c$  are the ‘‘bare’’ atomic states and the matrix elements are computed using the traditional inner products)

$$\begin{aligned} E_a^{(3)}(\omega) &= T_a(\omega) + C_a(\omega) + B_a(\omega) + O_a(\omega), \\ T_a(\omega) &= \sum_{b,c \neq a} \frac{(V_{\text{HFI}})_{ab}v_{bc}^{(+)}v_{ca}^{(-)}}{(E_b^{(0)} - E_a^{(0)})(E_c^{(0)} - \omega - E_a^{(0)})} + \sum_{b,c \neq a} \frac{(V_{\text{HFI}})_{ab}v_{bc}^{(-)}v_{ca}^{(+)}}{(E_b^{(0)} - E_a^{(0)})(E_c^{(0)} + \omega - E_a^{(0)})}, \\ C_a(\omega) &= \sum_{b,c \neq a} \frac{v_{ab}^{(+)}(V_{\text{HFI}})_{bc}v_{ca}^{(-)}}{(E_b^{(0)} - \omega - E_a^{(0)})(E_c^{(0)} - \omega - E_a^{(0)})} + \sum_{b,c \neq a} \frac{v_{ab}^{(-)}(V_{\text{HFI}})_{bc}v_{ca}^{(+)}}{(E_b^{(0)} + \omega - E_a^{(0)})(E_c^{(0)} + \omega - E_a^{(0)})}, \\ B_a(\omega) &= [T_a(\omega)]^*, \\ O_a(\omega) &= -(V_{\text{HFI}})_{aa} \sum_{b \neq a} \frac{v_{ab}^{(+)}v_{ba}^{(-)}}{(E_b^{(0)} - \omega - E_a^{(0)})^2} - (V_{\text{HFI}})_{aa} \sum_{b \neq a} \frac{v_{ab}^{(-)}v_{ba}^{(+)}}{(E_b^{(0)} + \omega - E_a^{(0)})^2}. \end{aligned}$$

We refer to  $T_a(\omega)$ ,  $C_a(\omega)$ , and  $B_a(\omega)$  contributions as the top, center, and bottom diagrams, respectively. The naming convention reflects the position of the HFI in the diagram.  $O_a(\omega)$  combines other, corrective terms; for the case at hand the  $O_a(\omega)$  term is irrelevant since the expectation value  $(V_{\text{HFI}})_{aa} = 0$  for  $J = 0$  states.

We carry out the angular reduction of these diagrams. We find that the magnetic-dipole HFI does not bring in neither the scalar nor the tensor contribution: there is only the vector component of the a.c. polarizability. In principle, the tensor contribution to  $J = 0$  polarizability might appear due to the electric-quadrupole moment of the nucleus; the strength of this interaction is typically two orders of magnitude smaller than that of the magnetic HFI and we neglect this effect. The final result simplified for the  $J = 0$  states reads

$$\delta E_a = - \left( \frac{1}{2} \mathcal{E} \right)^2 \mathcal{A} \alpha_{\gamma F}^A(\omega) \frac{M_F}{2I},$$

$M_F$  being the projection of  $F$  (i.e., the projection of the nuclear spin  $I$  for  $J = 0$ ). The conventional degree of the circular polarization is defined in terms  $\mathcal{A} = \sin 2\theta$  for an electromagnetic wave  $\mathcal{E} = \mathcal{E} \mathbf{e}_x \cos \theta \cos(\omega t - kz) + \mathcal{E} \mathbf{e}_y \sin \theta \sin(\omega t - kz)$ . The shift is expressed in terms of the vector polarizability

$$\alpha_{\gamma F}^A(\omega) = -\sqrt{\frac{2}{27}} \left\{ C_{1,1}^{(1)}(\gamma J, \omega) + 2T_{1,1}^{(1)}(\gamma J, \omega) \right\},$$

where the dynamic reduced sums are expressed in terms of the reduced matrix elements of the dipole operator and the HFI coupling

$$T_{J', J''}^{(K)}(\gamma J, \omega) = \mu_I \sum_{\gamma'} \sum_{\gamma'' \neq \gamma'} \langle \gamma J || T^{(1)} || \gamma'' J'' \rangle \langle \gamma'' J'' || D || \gamma' J' \rangle \langle \gamma' J' || D || \gamma J \rangle \times \\ \left( \frac{1}{E - E''} \frac{1}{E - E' + \omega} + (-1)^K (\omega \rightarrow -\omega) \right),$$

$$C_{J', J''}^{(K)}(\gamma J, \omega) = \mu_I \sum_{\gamma' \gamma''} \langle \gamma J || D || \gamma' J' \rangle \langle \gamma' J' || T^{(1)} || \gamma'' J'' \rangle \langle \gamma'' J'' || D || \gamma J \rangle \times \\ \left( \frac{1}{E - E' + \omega} \frac{1}{E - E'' + \omega} + (-1)^K (\omega \rightarrow -\omega) \right).$$

In these formulas  $E$  is the energy of the state of interest. Notation  $(-1)^K (\omega \rightarrow -\omega)$  means that the preceding term is multiplied by  $(-1)^K$  and  $\omega$  is replaced by  $-\omega$ . For  $J = 0$ , the selection rules require  $J' = J'' = 1$  for both reduced sums.

Analyzing these expressions numerically in the CI+MBPT approach, we find that the vector polarizability of the  $6^3P_0$  state of Yb is much larger than that for the ground state, as in the case of Sr [58]. For Sr, Katori et al. [58] estimated the vector polarizability by adding HFS correction to the energy levels of intermediate states. Our analysis is more complete and we find that the dominant effect is not due to corrections to the energy levels, but it is rather due to perturbation of the  $6^3P_0$  state by the HFS operator. The resulting values of  $\alpha_{6^3P_0}^A(\omega^*)$  are  $-0.10$  a.u. for  $^{171}\text{Yb}$  and  $0.075$  a.u. for  $^{173}\text{Yb}$ . Experimentally this translates to requiring  $\mathcal{A} < 10^{-6}$  at laser intensities of  $10 \text{ kW/cm}^2$  for keeping the induced clock shifts below the mHz level.

## VI. ZEEMAN EFFECT

When an atom is placed in the magnetic field, magnetic moments of its electrons and nuclei interact with the magnetic field, leading to the familiar Zeeman effect. The advantage of the  $J = 0$  levels used in the lattice clocks is that because of their scalar nature, to the lowest order in the field strength, they are not Zeeman-shifted. However, if we include the nuclear spin into the analysis, the linear Zeeman shift does appear, because the total angular momentum  $F$  no longer vanishes in general. Qualitatively, the linear Zeeman shift appears for  $I \neq 0$  because of the nuclear magnetic moment. This moment contributes both directly (through the coupling of the magnetic moment with the B-field) and indirectly. The indirect contribution is due to the mechanism of the HFI mixing which brings in contribution of  $J \neq 0$  levels with a large electronic magnetic moment. The two corrections are of the same order of magnitude.

We will present the discussion in terms of the so-called Lande g-factors  $g_F$ . It is introduced by considering the lowest-order perturbation by a sufficiently weak B-field,

$$\delta E_{M_F} = \langle F M_F | H_B | F M_F \rangle = \mu_B g_F B M_F,$$

the direction of the B-field being chosen as the quantization axis.

The direct contribution of the nuclear moment to the atomic g-factor is well known (see, e.g., Ref.[61]). For the  $J = 0$  level it simplifies to

$$\delta g_{F=I}^n = -\frac{1}{I} \left( \frac{m_e}{m_p} \right) \left( \frac{\mu_I}{\mu_N} \right),$$

and involves the ratio of the electron and proton masses. The ratio  $\mu_I/\mu_N$  is simply the nuclear magnetic moment expressed in nuclear magnetons. Notice that the textbook derivation of the above expression implies that the magnetic field acting on the nuclear magnetic moment is the same as the externally applied field. Generally this is not the case, as the currents induced inside the atom by external fields tend to shield the fields. This effect is usually parameterized in terms of the shielding constant  $\sigma$ :  $B_{\text{nuc}} = (1 - \sigma)B_{\text{external}}$ . Values for the shielding factors  $\sigma$  for closed-shell are listed in Ref. [62], indicating that the  $\delta g_{F=I}^n$  may be modified by as much as a few per cent. The shielding depends on the electronic state and should be different for the two clock states. This parallels the ‘‘chemical shift’’ effect in nuclear magnetic resonance. We are not aware of evaluation of the shielding correction for any of the atoms of interest to the lattice clocks. Considering that even the current clock experiments [63] can measure the differential g-factors to a 0.5%-level accuracy, such calculations may become of relevance.

Now we turn to the indirect contribution of the nuclear magnetic moment to the atomic g-factor. We consider an atom placed in the uniform magnetic field  $\mathbf{B}$ . The vector potential due to this field  $\mathbf{A} = (\mathbf{B} \times \mathbf{r})/2$  determines the coupling

$$H_B = (\boldsymbol{\alpha} \cdot \mathbf{A}) = \sum_{\lambda} (-1)^{\lambda} \mathcal{S}_{\lambda}^{(1)} B_{-\lambda},$$

with the irreducible tensor operator of rank 1 defined as

$$\mathcal{S}_{\lambda}^{(1)} = \frac{i}{\sqrt{2}} \left( \boldsymbol{\alpha} \cdot \mathbf{C}_{1\lambda}^{(0)}(\hat{\mathbf{r}}) \right).$$

Nonrelativistically, the interaction  $H_B$  reduces to

$$H_B^{(NR)} = \mu_B \mathbf{B} \cdot (\mathbf{L} + g_e \mathbf{S}), \quad (34)$$

where  $g_e \approx 2.0023$  is the g-factor of the electron (the quoted value also includes radiative QED corrections which are beyond the present consideration).

Neglecting coupling of the nuclear spin to the B-field, we obtain

$$g_F^e = \frac{1}{\mu_B M_F} \langle FM_F | \mathcal{S}_0^{(1)} | FM_F \rangle.$$

Non-vanishing correction to the g-factor arises due to HFI induced admixture to wave functions. This is the same mechanism that causes the  ${}^3P_0$  state to decay radiatively (see Section IV). The first-order correction  $|(IJ); FM_F\rangle^{(1)}$  to the wave function is given by Eq.(26), leading to the correction to the g-factor

$$\delta g_F^e \mu_B M_F = 2 \sum_{\gamma' J'} \frac{\langle \gamma(IJ); FM_F | \mathcal{S}_0^{(1)} | \gamma'(IJ'); FM_F \rangle \langle \gamma'(IJ'); FM_F | H_{\text{HFI}} | \gamma(IJ); FM_F \rangle}{E(\gamma' J') - E(\gamma J)}$$

When restricting the summation over intermediate states we took into account the scalar character of  $H_{\text{HFI}}$ . The operator  $\mathcal{S}_{\lambda}^{(1)}$  involves only electronic degrees of freedom; this restricts the intermediate electronic momentum to  $|J-1| \leq J' \leq J+1$ . For the  $J=0$  state,  $F=I$  and the non-vanishing HFI matrix element

$$\langle (I, J=1); FM_F | H_{\text{HFI}} | (I, J=0); FM_F \rangle = \left( \frac{\mu_I}{\mu_N} \right) \left( \frac{I+1}{3I} \right)^{1/2} \frac{\alpha}{2m_p} \langle \gamma' J' = 1 | | \mathcal{T}^{(1)} | | {}^3P_0 \rangle.$$

The matrix elements of the interaction with the external B-field is most easily evaluated in the nonrelativistic approximation. The nonrelativistic operator is diagonal with respect to the radial part of the wave function, implying that the only intermediate state that would admix to the  $nsnp$   ${}^3P_0$  state is the state  $nsnp$   ${}^3P_1$  of the same fine-structure multiplet. This leads to

$$\delta g_F^e = -\frac{2\sqrt{2}}{3I} (g_e - 1) \left( \frac{\mu_I}{\mu_N} \right) \frac{\alpha}{2m_p} \frac{\langle nsnp {}^3P_1 | | \mathcal{T}^{(1)} | | nsnp {}^3P_0 \rangle}{E(nsnp {}^3P_1) - E(nsnp {}^3P_0)}. \quad (35)$$

While using this expression, one should be careful with the relative phase convention between the  ${}^3P_1$  and  ${}^3P_0$  states: both states are assumed to nominally arise from the traditional coupling of  $S$  and  $L$  to their respective  $J$  with the same radial part of the total wave function. We emphasize that Eq.(35) was obtained using the nonrelativistic expression for the B-field coupling, Eq.(34), while the relativistic calculations are required for the HFI coupling which is primarily accumulated near the nucleus.

Now we illustrate the above formulas with numerical estimates for Yb. Here the CI+MBPT value of the HFI matrix element is  $\frac{\alpha}{2m_p} \langle {}^3P_1 || \mathcal{T}^{(1)} || {}^3P_0 \rangle = 6522$  MHz and the fine-structure splitting has the value of  $703.6$   $\text{cm}^{-1}$ . Numerical results for the nuclear  $\delta g_F^n$  and the electronic  $\delta g_F^e$  corrections to the g-factor are given in Table VII. One should observe that both corrections are of a comparable size. When analyzing the *differential* g-factors for the clock transition, one should keep in mind that  $\delta g_F^n$  factors are essentially the same for the ground and the excited state (the only difference is due to the ‘‘chemical shift’’ for the two levels), while in the nonrelativistic approximation the  $g_F^e$  of the ground state vanishes. The computed values imply that mHz shifts would be produced by  $\mu\text{G}$  magnetic fields. Fields can readily be calibrated and stabilized to this level using magnetic shielding.

TABLE VII: Lande g-factors for the  ${}^3P_0$  state of fermionic isotopes of Yb. The values are from Ref. [3].  $\delta g_F^n$  are the nuclear and  $\delta g_F^e$  are the electronic corrections, respectively. The total,  $\delta g$ , is the sum of the two g-factors.

Isotope	$\mu_I/\mu_N$	$I$	$\delta g_F^e$	$\delta g_F^n$	$\delta g_{\text{Total}}$
171	0.4919	1/2	$-2.9 \times 10^{-4}$	$-5.4 \times 10^{-4}$	$-8.3 \times 10^{-4}$
173	-0.6776	5/2	$7.9 \times 10^{-5}$	$+1.48 \times 10^{-4}$	$2.27 \times 10^{-4}$

## VII. BLACK-BODY RADIATION SHIFT

Considering advantages of optical lattice clocks, here we investigate an important systematic effect of the black-body radiation (BBR) on the frequency of the  ${}^3P_0 - {}^1S_0$  clock transition. Indeed, the current SI definition of the second explicitly involves atomic clock operating at the absolute zero of temperature [64]. While the present definition of the second is based on the microwave Cs clock, one may anticipate that the rapidly-progressing optical lattice clocks may be used to redefine the unit of time in the future. Beyond the metrologically-important BBR correction to the clock frequency, the BBR shifts also affect the error balance of the clocks: the non-uniform distribution of the temperature inside the clock chamber may lead to the effective broadening of the lines [2, 63].

In a laboratory environment with an ambient temperature  $T$ , one needs to introduce the  $T$ -dependent BBR correction to the observed frequency. Even in Cs the value of the BBR shift was a subject of a recent controversy [65–67]. Here we setup the relativistic multipolar theory of the BBR shifts and using techniques of many-body relativistic atomic structure, we compute the BBR shift for Mg, Ca, Sr, and Yb and evaluate uncertainties of the calculations. This Section is based on our paper [44] and provides additional details.

As summarized in Table VIII, the resulting fractional uncertainties in the clock frequencies at  $T = 300$  K are *large*, ranging from  $1 \times 10^{-17}$  for Mg to  $3 \times 10^{-16}$  for Yb.

The main conclusions of this Section are (i) the present uncertainty in our computed BBR shift is an obstacle on the way towards the projected  $10^{-18}$  accuracy goal; (ii) due to  $T^4$  scaling of the BBR shift, it may be beneficial to operate at cryogenic temperatures; (iii) if operating at room temperatures, high-precision (0.02%-accurate for Sr) measurements of the BBR shifts or related quantities are required; (iv) Mg-based clock is the least susceptible to BBR; compared to Sr, the Mg BBR shift is an order of magnitude smaller (see Table VIII). Additionally, we develop a general relativistic theory of the BBR shift caused by multipolar components of the radiation field.

TABLE VIII: Black-body radiation shift for clock transitions between the lowest-energy  ${}^3P_0$  and  ${}^1S_0$  states in divalent atoms.  $\delta\nu_{\text{BBR}}$  is the BBR shift at  $T = 300$  K with our estimated uncertainties.  $\nu_0$  is the clock transition frequency, and  $\delta\nu_{\text{BBR}}/\nu_0$  is the fractional contribution of the BBR shift. The last column lists fractional errors in the absolute transition frequencies induced by the uncertainties in the BBR shift.

Atom	$\delta\nu_{\text{BBR}}$ , Hz	$\nu_0$ , Hz	$\delta\nu_{\text{BBR}}/\nu_0$	uncertainty
Mg	-0.258(7)	$6.55 \times 10^{14}$	$-3.9 \times 10^{-16}$	$1 \times 10^{-17}$
Ca	-1.171(17)	$4.54 \times 10^{14}$	$-2.6 \times 10^{-15}$	$4 \times 10^{-17}$
Sr	-2.354(32)	$4.29 \times 10^{14}$	$-5.5 \times 10^{-15}$	$7 \times 10^{-17}$
Yb	-1.25(13)	$5.18 \times 10^{14}$	$-2.4 \times 10^{-15}$	$3 \times 10^{-16}$

### A. Multipolar theory of the black-body radiation shift

The BBR shift is caused by perturbation of the atomic energy levels by the oscillating thermal radiation. Both atomic levels involved in the clock transition are perturbed and the overall BBR correction is a difference of the BBR shifts for the two levels. We find that determining shift for the upper  ${}^3P_0$  level requires certain care. This level is a part of the  ${}^3P_J$  fine-structure manifold,  $J = 0, 1, 2$ . The separation between the levels in the manifold is comparable to the characteristic wavenumber of the BBR radiation,  $208.51 \text{ cm}^{-1}$ , at  $T = 300 \text{ K}$ , and contributions of the BBR-induced magnetic-dipole and electric-quadrupole transitions to the levels of the manifold may be enhanced. Taking these induced transitions into account requires going beyond the conventional electric-dipole approximation, Ref. [68].

Considering a potential importance of the multipolar contributions, here we derive the relevant formulas for BBR-induced energy shifts. Although we show that the M1 and E2 contributions can be neglected at the present level of uncertainty for the dominant E1 shift, incorporating M1 multipoles will be required if the lattice-clocks reach their projected  $10^{-18}$  accuracy level.

We start with the usual box quantization for the photon field and expand the magnetic potential inside the box of side  $L$  over the plane waves (see, e.g. Ref.[69])

$$\mathbf{A}(\mathbf{r}, t) = \sum_{\lambda} q_{\lambda} \mathbf{A}_{\lambda} e^{-i\omega_{\lambda} t} + c.c.$$

with

$$\mathbf{A}_{\lambda} = \frac{1}{L^{3/2}} \boldsymbol{\varepsilon}_{\lambda} e^{i(\mathbf{k}_{\lambda} \cdot \mathbf{r})}.$$

A periodic boundary condition is imposed on  $\mathbf{A}(\mathbf{r}, t)$ , effectively quantizing the modes,  $k_{\lambda} = \omega_{\lambda}/c$ . In the Gaussian units and the Coulomb gauge, the electron-field interaction Hamiltonian reads

$$H' = (\boldsymbol{\alpha} \cdot \mathbf{A}) = \frac{1}{L^{3/2}} \sum_{\lambda} q_{\lambda} v_{\lambda}^{(-)} e^{-i\omega_{\lambda} t} + \frac{1}{L^{3/2}} \sum_{\lambda} q_{\lambda}^* v_{\lambda}^{(+)} e^{+i\omega_{\lambda} t}$$

with  $v_{\lambda}^{(\pm)} = (\boldsymbol{\alpha} \cdot \boldsymbol{\varepsilon}_{\lambda}) e^{\mp i(\mathbf{k}_{\lambda} \cdot \mathbf{r})}$ . We are interested in the time-evolution of atomic states caused by these oscillating fields. To this end we expand the atomic wave function  $\psi(t)$  over the complete set of stationary states  $|k\rangle$  of the atom

$$|\psi(t)\rangle = \sum_k c_k(t) e^{-iE_k t} |k\rangle,$$

where the time-dependent amplitudes satisfy a set of coupled equations

$$i \frac{d}{dt} c_k(t) = \sum_p e^{i\omega_{kp} t} H'_{kp}(t) c_p(t).$$

Here  $\omega_{kp} = E_k - E_p$  and  $H'_{kp} \equiv \langle k | H' | p \rangle$  are the matrix elements of the Hamiltonian  $H'$ .

To solve this set of equations we employ the secular approximation. Indeed, the perturbing field is weak and we assume that it does not lead to large population transfer from the initial (perturbed) state  $\psi_g(t)$ . On the r.h.s. of the equation for the excited (perturbing) state amplitude we may neglect contributions of other excited states

$$i \frac{d}{dt} c_{k \neq g}(t) \approx e^{i\omega_{kg} t} H'_{kg}(t) c_g(t) = \frac{1}{L^{3/2}} \sum_{\lambda} \left\{ q_{\lambda} \left[ v_{\lambda}^{(-)} \right]_{kg} e^{i(\omega_{kg} - \omega_{\lambda}) t} + q_{\lambda}^* \left[ v_{\lambda}^{(+)} \right]_{kg} e^{i(\omega_{kg} + \omega_{\lambda}) t} \right\} c_g(t).$$

We expect that the reference state amplitude follows  $c_g(t) = c_g(0) \exp[-i\delta E_g t]$ , where the light shift  $\delta E_g \ll (\omega_{kg} \pm \omega_{\lambda})$ . Under this assumption we may disregard the time-dependence of  $c_g(t)$  while integrating the above equations. The resulting amplitudes for the excited states adiabatically follow the reference state amplitude

$$c_{k \neq g}(t) = X_{kg} c_g(t),$$

$$X_{kg} = \frac{1}{L^{3/2}} \sum_{\lambda} \left\{ q_{\lambda} \frac{\left[ v_{\lambda}^{(-)} \right]_{kg}}{\omega_{gk} + \omega_{\lambda}} e^{i(\omega_{kg} - \omega_{\lambda}) t} + q_{\lambda}^* \frac{\left[ v_{\lambda}^{(+)} \right]_{kg}}{\omega_{gk} - \omega_{\lambda}} e^{i(\omega_{kg} + \omega_{\lambda}) t} \right\}$$

We substitute this solution into the time-dependent equation for the  $c_g(t)$  amplitude, arriving at

$$i \frac{d}{dt} c_g(t) = \delta E_g c_g(t),$$

$$\delta E_g = \sum_k e^{i\omega_{gk}t} H'_{gk}(t) X_{kg}.$$

As a next step we carry out statistical averaging of the above expression over the field amplitudes  $q_\lambda$  and  $q_\lambda^*$ . The only non-vanishing combinations are

$$\langle q_\lambda q_\lambda^* \rangle = \frac{2\pi}{\alpha^2} \frac{1}{\omega_\lambda} \bar{n}_{\omega_\lambda},$$

where the mean occupation number for photons

$$\bar{n}_\omega = \frac{1}{\exp(\omega/T) - 1}.$$

Therefore,

$$\delta E_g = \frac{\alpha}{4\pi^2} \text{P.V.} \int_0^\infty d\omega \omega \bar{n}_\omega \sum_\varepsilon \int d\Omega_k \sum_p \left\{ \frac{[v^{(+)}]_{gp} [v^{(-)}]_{pg}}{\omega_{gp} + \omega} + \frac{[v^{(-)}]_{gp} [v^{(+)}]_{pg}}{\omega_{gp} - \omega} \right\},$$

where we made a transition  $\sum_\lambda \rightarrow \left(\frac{L}{2\pi}\right)^3 \sum_\varepsilon \int \int d\Omega_k k^2 dk$  in the limit of  $L \rightarrow \infty$ . P.V.  $\int d\omega$  stands for the Cauchy's principal value of the integral; as elucidated in Ref. [68] it is required for a proper treatment of nominally divergent resonant contributions.

So far the derivation paralleled the method discussed, for example, in Ref. [68] for the electric-dipole transitions. At this point we focus on multipolar fields. While evaluating matrix elements of operators  $v^{(\pm)}$ , we make use of the multipolar expansion of  $\varepsilon e^{i(\mathbf{k}\cdot\mathbf{r})}$  in vector spherical harmonics

$$\varepsilon e^{i(\mathbf{k}\cdot\mathbf{r})} = 4\pi \sum_{JM\lambda} i^{J-\lambda} \left( \mathbf{Y}_{JM}^{(\lambda)}(\hat{\mathbf{k}}) \cdot \varepsilon \right) \mathbf{a}_{JM}^{(\lambda)}(\mathbf{r}),$$

where  $\lambda = 0$  is for magnetic (MJ) and  $\lambda = 1$  is for electric (EJ) multipolar amplitudes (see Section III). To simplify the light-shift expression we employ the following property of the harmonics

$$\sum_\varepsilon \int d\Omega_k \left( \mathbf{Y}_{J'M'}^{(\lambda')*}(\hat{\mathbf{k}}) \cdot \varepsilon \right) \left( \mathbf{Y}_{JM}^{(\lambda)}(\hat{\mathbf{k}}) \cdot \varepsilon \right) = \delta_{JJ'} \delta_{\lambda\lambda'} \delta_{MM'},$$

As a result, we find that the BBR shift is a sum over independent multipolar contributions

$$\delta E_g = \sum_{J\lambda} \delta E_g^{(J\lambda)}, \quad (36)$$

where  $\lambda = 0$  is for magnetic (MJ) and  $\lambda = 1$  is for electric (EJ) multipolar amplitudes. The individual multipolar shifts are

$$\delta E_g^{(J\lambda)} = -\pi \frac{J+1}{J[(2J-1)!!]^2} \alpha^{2(J-1)} \text{P.V.} \int_0^\infty d\omega \omega^{2(J-1)} u_\omega(T) \bar{\alpha}_g^{(J\lambda)}(\omega). \quad (37)$$

Here  $\alpha_g^{(J\lambda)}(\omega)$  are the generalized dynamic multipolar scalar polarizabilities

$$\bar{\alpha}_g^{(J\lambda)}(\omega) = \frac{2}{2J+1} \sum_{p,M} |\langle p | Q_{JM}^{(\lambda)} | g \rangle|^2 \left\{ \frac{\omega_{pg}}{\omega_{pg}^2 - \omega^2} \right\}. \quad (38)$$

Here the transition operator was expressed in terms of the multipole moments  $q_{JM}^{(\lambda)}$  of Sec. III. The polarizabilities  $\bar{\alpha}_g^{(J\lambda)}(\omega)$  are proportional to the scalar polarizabilities, Eq.(23) of Section III. Here for convenience we pulled out frequency-dependent prefactor for clarifying the following derivation.

A cursory examination of Eqs.(37,38) reveals that compared to  $2^J$  multipole, the contribution of  $2^{J+1}$  multipole is suppressed by a factor of  $\alpha^2$ . Also for the same  $J$  the magnetic contribution is  $\alpha^2$  weaker than that of the EJ photons. As in the theory of multipolar radiative transitions E(J+1) and MJ contributions are of the same order in  $\alpha$ . To illuminate the  $T$ -dependence of contributions of individual intermediate states we recast the BBR shifts into a form ( $J_g$  is the total angular momentum of the reference state,  $\langle g||q_{JM}^{(\lambda)}||p\rangle$  is the reduced matrix element, and we separate out factor of  $\alpha^2$  for MJ matrix elements )

$$\delta E_g^{(\lambda J)} = -\frac{(\alpha T)^{2J+1}}{2J_g + 1} (\alpha^2)^{\lambda-1} \sum_p (\alpha^2)^{1-\lambda} \left| \langle g||Q_J^{(\lambda)}||p\rangle \right|^2 F_J \left( \frac{\omega_{pg}}{T} \right), \quad (39)$$

with universal functions ( $x = \omega/T$ )

$$F_J(y) = \frac{1}{\pi} \frac{J+1}{J(2J+1)!!(2J-1)!!} P.V. \int_0^\infty \left( \frac{1}{y+x} + \frac{1}{y-x} \right) \frac{x^{2J+1}}{e^x - 1} dx. \quad (40)$$

The universal functions  $F_J(y)$  are multipolar generalizations of function  $F(y)$  introduced by Farley and Wing [68] in the E1 case. We computed  $F_J$  functions using standard integration routines built-in into Mathematica. A plot of  $F_J(y)$  for several  $J$  may be found in Ref. [44].  $F_J$  rapidly change around  $y \sim 1$  and slowly fall off for  $y \gg 1$ . Depending on the value of excitation energy,  $\omega_{pg} = yT$ , a particular intermediate state may introduce either negative or positive BBR shift.  $F_J$  are broad distributions and have comparable values for  $|y| \lesssim 20$ .

The limit  $y \gg 1$  corresponds to the case when the transition energy is much larger than  $T$ . Here  $|y| \gg 1$ ,  $F_J(y) \propto 1/y$ . If all virtual transitions satisfy this requirement, then the leading contribution to the multipolar BBR shift can be expressed in terms of static polarizabilities

$$\delta E_g^{(J\lambda)} = -\frac{\zeta(2J+2)(2J+2)!}{2\pi J[(2J-1)!!]^2} \alpha^{2J+1} T^{2J+2} \bar{\alpha}_g^{(J\lambda)}(0), \quad (41)$$

where  $\zeta$  is the Riemann zeta-function. As the scaling factor,  $\alpha^{2J+1} T^{2J+2}$ , is expressed in atomic units, we observe that as multipolarity  $J$  increases by one, in addition to the usual  $\alpha^2$  suppression, there is a temperature suppression factor of  $(k_B T/E_h)^2$ . For  $T = 300$  K this suppression is sizable, as  $(k_B T/E_h)^2 \approx 9.0 \times 10^{-7}$ .

## B. BBR shift for the clock transition in divalent atoms

Below we apply the developed formalism to computing the BBR shift for the  $^1S_0 - ^3P_0$  clock transition in divalent atoms. We will assume that the atoms are at the ambient temperature of  $T = 300$  K. Both clock levels experience the BBR shift and the total shift is the difference between the individual shifts,  $\delta\nu_{\text{BBR}} = \delta\nu_{\text{BBR}}(^3P_0) - \delta\nu_{\text{BBR}}(^1S_0)$ .

Consider first the BBR shift of the ground  $^1S_0$  state. Here transition energies of various multipolar transitions to the upper levels are much larger than  $T$ , i.e., we are in the  $y \gg 1$  limit. Here compared to the dominant E1-induced shift, the contribution of M1 transitions is suppressed by  $\alpha^2 \sim 10^{-4}$  and E2 by  $\alpha^2 (k_B T/E_h)^2 \sim 10^{-10}$ . Higher-order multipoles are suppressed even more. As to the retardation effects in E1 matrix elements, we expect that they would be suppressed by a factor of  $\alpha^2 (k_B T/E_h)^2 \sim 10^{-10}$ . Nevertheless, since the fractional contribution of the BBR shift to the clock frequency is at  $5 \times 10^{-15}$  level (see Table VIII), one would need to introduce the M1 corrections at the projected accuracy of  $10^{-18}$ .

For the  $^3P_0$  levels, the characteristic thermal photon frequency is comparable to the fine-structure intervals for the  $^3P_J$  manifold. The  $^3P_0$  level is connected by M1 transition to the  $^3P_1$  level and by E2 transition to the  $^3P_2$  level. For these transitions the values of the relevant functions  $F_J \sim 1$ , thus  $\delta E_g^{(M1)} \sim \alpha^2 (\alpha T)^3$ ,  $\delta E_g^{(E2)} \sim (\alpha T)^5$ , while  $\delta E_g^{(E1)} \sim \alpha^3 (T)^4 / \omega_{3D_1-3P_0}$ . Qualitatively, we anticipate that M1 and E2 contributions are suppressed by factors of  $10^{-3}$  and  $10^{-11}$ , respectively. (Notice that  $\omega_{3D_1-3P_0} \approx 2 \times 10^{-2} E_h$ .) Our numerical estimate, based on the transitions inside the fine-structure manifold lead to the following values of the BBR shifts for Sr:  $\delta E_g^{(M1)} = 2.4 \times 10^{-5}$  Hz and  $\delta E_g^{(E2)} = 2.5 \times 10^{-8}$  Hz. Since the E1 BBR shift for Sr is  $\sim 2$  Hz, the M1 and E2 contributions can be neglected at the present 1%-level of accuracy of our calculations.

We find that although the thermal photon energy is close to the fine-structure intervals, the induced multipole BBR shifts are not amplified. The main reason is that the BBR energy distribution is broad: the functions  $F_J$  have comparable values for a wide range of excitation energies,  $|\omega| \lesssim 20T$ . For example, for Sr  $^3P_0 - ^3D_1$  E1 transition  $F_1 \approx 0.16$ , while for the  $^3P_0 - ^3P_1$  M1 transition  $F_1 \approx -0.41$  and for the  $^3P_0 - ^3P_2$  E2 transition  $F_2 \approx -0.36$ . For such a broad distribution, the multipolar BBR shift is determined by the prefactor in Eq. (39) resulting in a suppression of multipoles beyond E1.

Based on the above discussion, we may exclusively focus on the electric-dipole ( $J = 1, \lambda = 1$ ) contribution to the BBR shift. From our general expressions we obtain an approximate formula,

$$\delta E_g^{(E1)} \approx -\frac{2}{15}(\alpha\pi)^3 T^4 \alpha_g^{(E1)}(0) \times [1 + \eta], \quad (42)$$

$$\eta = \frac{(80/63)\pi^2}{\alpha_g^{(E1)}(0)T} \sum_p \frac{|\langle p || Q_1^{(1)} || g \rangle|^2}{(2J_g + 1)y_p^3} \left( 1 + \frac{21\pi^2}{5y_p^2} + \frac{336\pi^4}{11y_p^4} \right). \quad (43)$$

Here  $y_p = \omega_{pg}/T$  and  $\alpha_g^{(E1)}(0)$  is the traditional static dipole polarizability. To arrive at the above equation, we used asymptotic expansion

$$F_1(y) \approx \frac{4\pi^3}{45y} + \frac{32\pi^5}{189y^3} + \frac{32\pi^7}{45y^5} + \frac{512\pi^9}{99y^7},$$

which has an accuracy better than 0.1% for  $|y| > 10$ .  $\eta$  represents a “dynamic” fractional correction to the total shift.

### C. Numerical results

The leading contribution to the BBR shift is determined by the static E1 polarizability. We have evaluated them in Section II using a relativistic many-body procedure. The results of calculations for the static electric dipole polarizabilities for the  $ns^2\ ^1S_0$  and  $nsnp\ ^3P_0$  states were presented in Table V. The discussion of the accuracy of our results is given in Section II B.

With the computed polarizabilities we find the BBR shifts with Eq.(42). The “dynamic” correction  $\eta$  is negligible for the  $^1S_0$  states, but is needed for the  $^3P_0$  calculations. Indeed, for the ground state, the smallest excitation energy  $E_{1P_1} - E_{1S_0}$  is equal to 21698  $\text{cm}^{-1}$  for Sr. At  $T = 300\text{K}$  the characteristic value of  $y \sim 100$  for all the atoms. By contrast, for the  $^3P_0$  clock level, the transitions to the nearby  $^3D_1$  level (see Fig. 1) involve smaller energies. For Sr, the relevant energy is only 3841  $\text{cm}^{-1}$  corresponding to characteristic value of  $y \sim 20$ . At this value, the “static polarizability” approximation has only a few percent accuracy. While evaluating  $\eta$  we find it sufficient to truncate the summation over intermediate states at the lowest-energy excitation. This “dynamic” correction contributes to the BBR shift of the  $^3P_0$  state at 0.1% level in Mg, 1% in Ca, 2.7% in Sr, and 0.7% in Yb. Notice that since the clock BBR shift is obtained by subtracting BBR shifts of the individual levels, the “dynamic” correction contributes at an enhanced 5% level in Sr.

Finally, we combine the BBR shifts of the individual clock levels and arrive at the overall BBR corrections summarized in Table VIII. Our computed BBR shift for Sr,  $-2.354(32)$  Hz is in agreement with an estimate [2] of  $-2.4(1)$  Hz. The uncertainties are better than 3%, except for Yb where the uncertainty is 10%. These uncertainties are large compared to the projected  $10^{-18}$  fractional accuracy of the lattice-based clocks (see Table VIII).

At room temperatures, the uncertainties in BBR shifts seem to be a major factor in the error budget of these clocks. At the projected  $10^{-18}$  fractional accuracy, the required accuracies (e.g., 0.02% for Sr) in determining BBR shifts are beyond the presently demonstrated capabilities of atomic calculations and related polarizability measurements.

If any experimental (theoretical) progress is achieved (for instance, if sufficiently accurate values of the dipole matrix elements such as  $\langle ^3P_0 || D || ^3D_1 \rangle$  become available) the uncertainties in the BBR shifts due to E1-polarizabilities can be reduced. In this case the accurate calculation of the BBR shift contributions from M1- and E2-transitions will be needed using the formalism developed in this Section. At present the uncertainties of the E1-polarizabilities are so large that the projected  $10^{-18}$  fractional accuracy of the optical-lattice clocks seem to be difficult to attain (if the future definition of the second involves atoms at  $T = 0\text{K}$ ). In any case the BBR contribution has to be taken into account when evaluating uncertainties due to either spatial or temporal fluctuations of the thermal radiation.

## VIII. SUMMARY

In this Chapter we presented a detailed evaluation of a number of important atomic-structure parameters affecting design and ultimate accuracy of lattice clocks involving optical  $^3P_0 - ^1S_0$  transition in divalent atoms. The calculations were carried out using *ab initio* relativistic many-body methods of atomic structure. Overall we find that the calculations of this sort are reliable and the underlying formalism provides a clear systematic way on improving theoretical accuracy further. In particular, we evaluated the hyperfine-induced transition widths of the clock transitions, multipolar and vector a.c. polarizabilities, static polarizabilities, “magic” trapping wavelengths, hyperfine-induced g-factors, and black-body radiation shifts. Among the remaining parameters one of the important systematic effects

is due to hyperpolarizability, i.e., contribution to the Stark shifts *quartic* in the atom-laser interaction [58]. Evaluation of this quantity is discussed in details in Chapter **YYY** **Editor, please insert cross-reference to Palchikov's chapter.**

This work was supported in part by the US National Science Foundation, NIST precision measurement grant, and by the Russian Foundation for Basic Research under grant No 05-02-16914-a.

- 
- [1] H. Katori, in *Proc. 6th Symposium Frequency Standards and Metrology*, edited by P. Gill (World Scientific, Singapore, 2002), pp. 323–330.
- [2] M. Takamoto, F. L. Hong, R. Higashi, and H. Katori, *Nature (London)* **435**, 321 (2005).
- [3] S. G. Porsev, A. Derevianko, and E. N. Fortson, *Phys. Rev. A* **69**, 021403(R) (2004).
- [4] Jan W. Thomsen, private communication.
- [5] F. Riehle et al., talk at the Second Workshop on Cold Alkaline-Earth Atoms, September 11-13, 2003, Copenhagen, Denmark.
- [6] R. Santra, E. Arimondo, T. Ido, C. H. Greene, and J. Ye, *Phys. Rev. Lett.* **94**, 173002 (2005).
- [7] T. Hong, C. Cramer, W. Nagourney, and E. N. Fortson, *Phys. Rev. Lett.* **94**, 050801 (2005).
- [8] A. V. Taichenachev, V. I. Yudin, C. W. Oates, C. W. Hoyt, Z. W. Barber, and L. Hollberg, *Phys. Rev. Lett.* **96**, 083001 (2006).
- [9] C. Froese Fischer, G. Tachiev, and A. Irimia, *Atomic Nucl. Data Tables* **92**, 607 (2006).
- [10] R. Santra, K. V. Christ, and C. H. Greene, *Phys. Rev. A* **69**, 042510 (2004).
- [11] I. Lindgren and J. Morrison, *Atomic Many-Body Theory* (Springer-Verlag, Berlin, 1986), 2nd ed.
- [12] A. Derevianko and S. G. Porsev, *Theoretical overview of atomic parity violation. Recent developments and challenges* (2006), submitted to *Eur. J. Phys. A*, arXiv.org: hep-ph/0608178.
- [13] V. A. Dzuba, V. V. Flambaum, and M. G. Kozlov, *Phys. Rev. A* **54**, 3948 (1996).
- [14] V. A. Dzuba, M. G. Kozlov, S. G. Porsev, and V. V. Flambaum, *Zh. Eksp. Teor. Fiz.* **114**, 1636 (1998), [*Sov. Phys.-JETP* **84** 461, (1997)].
- [15] M. G. Kozlov and S. G. Porsev, *Eur. Phys. J. D* **5**, 59 (1999).
- [16] M. G. Kozlov and S. G. Porsev, *Opt. Spectrosc.* **87**, 384 (1999), [*Opt. Spectrosc.* **87** 352, (1999)].
- [17] S. G. Porsev, Yu. G. Rakhlina, and M. G. Kozlov, *J. Phys. B* **32**, 1113 (1999).
- [18] S. G. Porsev, Yu. G. Rakhlina, and M. G. Kozlov, *Phys. Rev. A* **60**, 2781 (1999).
- [19] M. G. Kozlov, S. G. Porsev, and I. I. Tupitsyn, *Phys. Rev. Lett.* **86**, 3260 (2001).
- [20] S. G. Porsev, M. G. Kozlov, Yu. G. Rakhlina, and A. Derevianko, *Phys. Rev. A* **64**, 012508 (2001).
- [21] M. G. Kozlov, S. G. Porsev, and W. R. Johnson, *Phys. Rev. A* **64**, 052107 (2001).
- [22] C. E. Moore, *Atomic energy levels*, vol. I-III (NBS, National Standards Reference Data Series – 35, U.S. GPO, Washington, D.C., 1971).
- [23] I. M. Savukov and W. R. Johnson, *Phys. Rev. A* **65**, 042503 (2002).
- [24] S. G. Porsev and A. Derevianko, *Phys. Rev. A* **69**, 042506 (2004).
- [25] A. Lurio, *Phys. Rev.* **126**, 1768 (1962).
- [26] M. Arnold, E. Bergmann, P. Bopp, C. Dorsch, J. Kowalski, T. Stehlin, and F. Trager, *Hyperfine Int.* **9**, 159 (1981).
- [27] P. Grundevik, M. Gustavsson, I. Lindgren, G. Olsson, L. Robertsson, A. Rosen, and S. Svanberg, *Phys. Rev. Lett.* **42**, 1528 (1979).
- [28] S. M. Heider and G. O. Brink, *Phys. Rev. A* **16**, 1371 (1977).
- [29] D. L. Clark, M. E. Cage, D. A. Lewis, and G. W. Greenlees, *Phys. Rev. A* **20**, 239 (1979).
- [30] B. Budick and J. Snir, *Phys. Rev.* **178**, 18 (1969).
- [31] A. Godone and C. Novero, *Phys. Rev. A* **45**, 1717 (1992).
- [32] W. W. Smith and A. Gallagher, *Phys. Rev.* **145**, 26 (1966).
- [33] H. S. Kwong, P. L. Smith, and W. H. Parkinson, *Phys. Rev. A* **25**, 2629 (1982).
- [34] L. Lundin, B. Engman, J. Hilke, and I. Martinson, *Phys. Scr.* **8**, 274 (1973).
- [35] D. Husain and C. J. Roberts, *J. Chem. Soc., Faraday Trans. 2* **82**, 1921 (1986).
- [36] C. Degenhardt, T. Binnewies, G. Wilpers, U. Sterr, F. Riehle, C. Lisdat, and E. Tiemann, *Phys. Rev. A* **67**, 043408 (2003).
- [37] R. Drozdowski, M. Ignasiuk, J. Kwela, and J. Heldt, *Z. Phys. D: At., Mol. Clusters* **41**, 125 (1997).
- [38] D. Husain and J. Schifino, *J. Chem. Soc., Faraday Trans. 2* **80**, 321 (1984).
- [39] M. Yasuda, T. Kishimoto, M. Takamoto, and H. Katori, *Phys. Rev. A* **73**, 011403 (2006).
- [40] C. J. Bowers, D. Budker, S. J. Freedman, G. Gwinner, J. E. Stalnaker, and D. DeMille, *Phys. Rev. A* **59**, 3513 (1999).
- [41] Y. Takasu, K. Komori, K. Honda, M. Kumakura, T. Yabuzaki, and Y. Takahashi, *Phys. Rev. Lett.* **93**, 123202 (2004).
- [42] R. M. Sternheimer, *Phys. Rev.* **80**, 102 (1950).
- [43] A. Dalgarno and J. T. Lewis, *Proc. R. Soc. London, Ser. A* **223**, 70 (1955).
- [44] S. G. Porsev and A. Derevianko, *Phys. Rev. A* **74**, 020502(R) (2006).
- [45] A. Derevianko, W. R. Johnson, M. S. Safronova, and J. F. Babb, *Phys. Rev. Lett.* **82**, 3589 (1999).
- [46] W. R. Johnson, *Adv. At. Mol. Opt. Phys.* **25**, 375 (1988).
- [47] S. G. Porsev and A. Derevianko, *Zh. Eksp. Teor. Fiz.* **129**, 227 (2006), [*Sov. Phys.-JETP* **102** 195, (2006)].

- [48] S. G. Porsev and A. Derevianko, *Phys. Rev. A* **65**, 020701(R) (2002).
- [49] J. Mitroy and M. W. J. Bromley, *Phys. Rev. A* **68**, 052714 (2003).
- [50] S. H. Patil, *Eur. Phys. J. D* **10**, 344 (2000).
- [51] A. Lurio and R. Novic, *Phys. Scr.* **134**, A608 (1964).
- [52] N. L. Manakov, V. D. Ovsianikov, and L. P. Rapoport, *Phys. Rep.* **141**, 319 (1986).
- [53] J. D. Bjorken and S. D. Drell, *Relativistic Quantum Mechanics* (1964).
- [54] V. B. Berestetskii, E. M. Lifshitz, and L. P. Pitaevskii, *Quantum Electrodynamics* (Pergamon Press, Oxford, 1982), 2nd ed.
- [55] W. R. Johnson, D. R. Plante, and J. Sapirstein, *Adv. At. Mol. Opt. Phys.* **35**, 255 (1995).
- [56] D. A. Varshalovich, A. N. Moskalev, and V. K. Khersonskii, *Quantum Theory of Angular Momentum* (World Scientific, Singapore, 1988).
- [57] Z. W. Barber, C. W. Hoyt, C. W. Oates, L. Hollberg, A. V. Taichenachev, and V. I. Yudin, *Phys. Rev. Lett.* **96**, 083002 (2006).
- [58] H. Katori, M. Takamoto, V. G. Pal'chikov, and V. D. Ovsianikov, *Phys. Rev. Lett.* **91**, 173005 (2003).
- [59] R. G. Garstang, *J. Opt. Soc. Am.* **52**, 845 (1962).
- [60] M. Yasuda and H. Katori, *Phys. Rev. Lett.* **92**, 153004 (2004).
- [61] H. Haken and W. H. C., *Physics of Atoms and Quanta* (Springer, 1994).
- [62] D. Kolb, W. R. Johnson, and P. Shorer, *Phys. Rev. A* **26**, 19 (1982).
- [63] M. M. Boyd, T. Zelevinsky, A. D. Ludlow, S. M. Foreman, S. Blatt, T. Ido, and J. Ye, *Science* **314**, 1430 (2006).
- [64] B. N. Taylor, ed., *The International System of Units (SI)* (U.S. Government Printing Office, Gaithersburg, Maryland USA, 2001).
- [65] F. Levi, D. Calonico, L. Lorini, S. Micalizio, and A. Godone, *Phys. Rev. A* **70**, 033412 (2004).
- [66] K. Beloy, U. I. Safronova, and A. Derevianko, *Phys. Rev. Lett.* **97**, 040801 (2006).
- [67] E. J. Angstrom, V. A. Dzuba, and V. V. Flambaum, *Phys. Rev. Lett.* **97**, 040802 (2006).
- [68] J. W. Farley and W. H. Wing, *Phys. Rev. A* **23**, 2397 (1981).
- [69] H. S. Friedrich, *Theoretical Atomic Physics* (Springer, Berlin, 2004), 2nd ed.